Photonuclear reactions on stable isotopes of cadmium and tellurium at bremsstrahlung end-point energies of 10−23 MeV*

F. A. Rasulova[1,2†] A. A. Kuznetsov[3,4] V. O. Nesterenko[5] J. H. Khushvaktov[2,6] S. I. Alekseev[1]
N.Yu. Fursova[3] A. S. Madumarov[1] I. Chuprakov[1,7] S. S. Belyshev[3,4] N. V. Aksenov[1]

[1]Flerov Laboratory of Nuclear Reactions of Joint Institute for Nuclear Research, Dubna, 141980 Russia
[2]Institute of Nuclear Physics of the Academy of Sciences of the Republic of Uzbekistan, Tashkent, 100214 Republic of Uzbekistan
[3]Skobeltsyn Institute of Nuclear Physics of Lomonosov Moscow State University, Moscow, 119234 Russia
[4]Faculty of Physics of Lomonosov Moscow State University, Moscow, 119991 Russia
[5]Bogoliubov Laboratory of Theoretical Physics of Joint Institute for Nuclear Research, Dubna, Russia
[6]Dzhelepov Laboratory of Nuclear Problems of Joint Institute for Nuclear Research, Dubna, 141980 Russia
[7]Institute of Nuclear Physics, Almaty, 050032 Republic of Kazakhstan

Abstract: In this study, the γ-activation approach was used to conduct tests at the bremsstrahlung end-point energies of 10−23 MeV by utilizing the MT-25 microtron beam. The experimental values of the relative yields and cross sections per equivalent quantum of photonuclear reactions on the stable isotopes of cadmium and tellurium were compared with the theoretical calculation results obtained from TALYS-2.0 using the default parameters and the combined model of photonucleon reactions (CMPR). The inclusion of isospin splitting in the CMPR allows for the definition of experimental data on the proton escape reactions with energies ranging from 17 to 23 MeV. Therefore, isospin splitting must be considered to accurately describe the decay of the giant dipole resonance. For Cd isotopes, essential discrepancies of yet unclear origin between theory (TALYS 2.0 and CMPR) and experimental data are found in the neutron channel.

Keywords: bremsstrahlung, cross section, cross section per equivalent quantum, isospin splitting, giant dipole resonance

DOI: 10.1088/1674-1137/ae551d **CSTR:** 32044.14.ChinesePhysicsC.50064003

I. INTRODUCTION

In order to learn more about how the population of nuclear shells affects unique aspects of the decay of excited nuclear states, it is interesting to investigate the photodisintegration of nuclei located close to the Z = 50 closed proton shell. The yields of different channels of the photodisintegration of isotopes in comparison with the ratio of the numbers of neutrons and protons in the nuclei can highlight the mechanisms of excitation and decay of nuclear states in the energy region between 10 and 50 MeV.

Cadmium (Z = 48) and tellurium (Z = 52) isotopes are suitable for investigations, as they have several stable isotopes under natural conditions, which allows to obtain the dependence of the yields of various reactions on the number of neutrons in a nucleus. The main decay channels of the giant dipole resonance (GDR) are the emission of neutrons or protons. Currently, an extensive database of experimental data on the photoneutron reactions in the stable isotopes of the natural mixture of cadmium and tellurium [1−22] is available. Nevertheless, these data are currently incomplete and lack a proper explanation. The proton channel, despite a small cross section of the (γ,p) reaction, is interesting in connection with the isospin splitting of the GDR [23].

Natural cadmium consists of eight stable isotopes with the following mass numbers and isotopic abundances: ^{106}Cd (1.25%), ^{108}Cd (0.89%), ^{110}Cd (12.49%), ^{111}Cd (12.80%), ^{112}Cd (24.13%), ^{113}Cd (12.22%), ^{114}Cd (28.73%), and ^{116}Cd (7.49%). The photoneutron reaction cross sections $\sigma(\gamma,n) + \sigma(\gamma, np)$ and $\sigma(\gamma, 2n)$ as well as the total absorption cross section $\sigma(\gamma, sn) = \sigma(\gamma,n) + \sigma(\gamma, np) + \sigma(\gamma, 2n)$ for a target from a natural mixture of cadmium isotopes were measured by using a beam of quasimonochromatic photons without separating the contributions from the reactions on individual isotopes [1]. The majority of photonuclear reaction data on cadmium isotopes

Received 26 November 2025; Accepted 19 March 2026; Accepted manuscript online 20 March 2026

* The work is supported by the National Research Foundation of South Africa, as well as the Joint Institute for Nuclear Research (Project No. 22, Radiochemistry, FLNR Part) and partially financed by the state budget of the Republic of Uzbekistan

† E-mail: rasulova@jinr.ru

have been obtained in experiments using bremsstrahlung photons. For example, the relative yields of multiparticle reactions on natural cadmium were studied using the end-point energy of 23 MeV [2, 3] and 55 MeV [4−6]; the flux-averaged cross section was determined using the end-point energies of 50 and 60 MeV [7]; isomeric ratios were determined using electron bremsstrahlung for the pairs ^{115m,g}Cd [7−15] and ^{104m,g}Ag [13].

Natural tellurium consists of eight stable isotopes with the following mass numbers and isotopic abundances: ^{120}Te (0.09%), ^{122}Te (2.55%), ^{123}Te (0.89%), ^{124}Te (4.74%), ^{125}Te (7.07%), ^{126}Te (18.84%), ^{128}Te (31.74%), and ^{130}Te (34.08%). Although all these isotopes can undergo photodisintegration via different reaction channels, only a few have been studied to date, such as photoneutron reactions [10−12,16−22]. The cross sections for the (γ, n) [22], (γ, n) + (γ, pn) [16] and (γ, $2n$) + (γ, $2np$) [16] reactions on the isotopes ^{120,124,126,128,130}Te induced by bremsstrahlung photons and positron annihilation in flight were determined by detecting neutrons in the energy range of the γ quantum (8.03−26.46 MeV). Isomeric ratios have been measured for the pairs ^{119m,g}Te [10, 17, 19, 20], ^{121m,g}Te [10, 11, 19, 20], ^{123m,g}Te [10, 18], ^{127m,g}Te [11,19, 21], and ^{129m,g}Te [10−12, 17,19, 21].

This study aimed to obtain new data on fundamental photonuclear reactions of cadmium and tellurium isotopes using a bremsstrahlung γ-radiation beam with energies between 10 and 23 MeV. We used TALYS-2.0 [24] and the combined model of photonucleon reactions (CMPR) [25] for simulations and the γ-activation method with bremsstrahlung photons from the electron accelerator to obtain our experimental data. Furthermore, the photoproton reaction product ^{111}Ag is a prospective medicinal isotope [26−29]; thus, examining the reaction yields is beneficial for both research and practical applications.

This paper is organized as follows. Sec. II describes the experimental set-up and procedures. Sec. III outlines the data analysis methods. In Sec. IV, the results for Cd and Te isotopes are presented and discussed. Sec. V presents the conclusions. Appendix A presents the tabulated experimental results, whereas Appendix B examines the TALYS options and GDR isospin splitting.

II. EXPERIMENTAL SET-UP AND PROCEDURES

This experiment was conducted using the output electron beam of the MT-25 microtron [30]. The electron energies ranged from 10 to 23 MeV, with an energy step of 1 MeV. Table 1 lists the main experimental parameters. A tungsten radiator target, a common convertor material, was used to generate the γ-radiation. The tungsten target was thick enough (3 mm) to maximize the amount of photons in the energy range of the GDR, which dominates the photonuclear cross section between the nucleon separation threshold and 20−30 MeV. To eliminate the leftover electrons from the bremsstrahlung beam, a 30 mm thick aluminum absorber was positioned behind the tungsten converter. The Cd and Te targets were located perpendicular to the electron beam and 1 cm away from the converter. The target of natural cadmium had dimensions 10 mm×10 mm×0.5 mm (at 10−19 MeV) and 5 mm×5 mm×0.5 mm (at 20−23 MeV). The natural tellurium target in powder form was enclosed in aluminum foils in the form of a square envelope with sizes of 15 mm×15

Table 1. Main parameters of the experiment.

Energy of electrons/MeV	Mass of targets/mg		Integral charge/mC		Irradiation time/min		Total measurement time of spectra/d	
	^{nat}Cd	^{nat}Te	^{nat}Cd	^{nat}Te	^{nat}Cd	^{nat}Te	^{nat}Cd	^{nat}Te
10	475	1050	50 (5)	30 (3)	97	100	1.8	3.9
11	448	1100	50 (5)	20 (2)	150	62	1.8	3.1
12	454	1010	50 (5)	10 (1)	125	32	1.8	3.8
13	451	1060	50 (5)	10 (1)	155	29	2.0	3.2
14	451	1080	30 (3)	4.0 (4)	175	50	1.6	3.6
15	414	1000	20 (2)	4.0 (4)	65	12	1.7	3.5
16	417	220	10 (1)	4.0 (4)	65	15	1.7	3.8
17	427	190	4.0 (4)	4.0 (4)	37	34	1.6	4.7
18	401	100	3.0 (3)	4.0 (4)	24	49	1.5	4.7
19	389	110	3.0 (3)	4.0 (4)	32	55	1.6	3.5
20	113	90	3.0 (3)	4.0 (4)	51	28	1.6	2.9
21	116	90	3.0 (3)	4.0 (4)	35	41	1.5	3.3
22	116	90	3.0 (3)	4.0 (4)	27	37	1.7	4.7
23	112	90	3.0 (3)	4.0 (4)	21	31	1.7	4.1

mm×2 mm (at 10−15 MeV), 8 mm×8 mm×2 mm (at 16−19 MeV), and 6 mm×6 mm×2 mm (at 20−23 MeV).

In the trials, a bremsstrahlung flux generated in the tungsten converter was utilized to irradiate the metallic natural cadmium and tellurium samples. The fluctuations in the beam current were measured using a Faraday cup and calibrated ionization chamber in the beam, and subsequently recorded in a web-accessible database for future analysis by using LabView software and an analog-to-digital converter card. [31]. Along with the Faraday cup and ionization chamber, the beam current was determined by digitizing the electrical charge accumulated on the target. During irradiation, the electron current of the accelerator was measured using a Faraday cup. A 0.15-mm-thick copper monitor was positioned behind the irradiation target. The absolute value of the current was calculated by comparing the experimentally measured and theoretical yields at the monitor based on the ^{65}Cu(γ, n)^{64}Cu reaction. The experimental cross sections of the partial photoneutron reactions for the ^{65}Cu nucleus, obtained on quasimonoenergetic annihilation photon beams [32] using the neutron multiplicity sorting method, display considerable systematic uncertainties and do not satisfy the specially introduced objective physical data reliability criteria. We applied the corrected theoretical cross sections, which were used to evaluate the cross sections of the partial reactions by employing the experimental-theoretical approach [33]. The yield of the ^{65}Cu(γ, n)^{64}Cu reaction was determined using the expected cross section [33], and the bremsstrahlung spectrum was generated using Geant4 [34].

Once the radiation levels in the experimental hall were safe, the targets were transferred to a different measurement room and the induced activity in the irradiated target was measured. We used a high purity germanium (HPGe) γ-detector with a resolution of 16 keV at 1332 keV, together with standard measurement electronics and a 16K ADC/MCA (Multiport II Multichannel Analyser, CANBERRA). The energy and efficiency of the HPGe detector were calibrated using standard γ-ray sources. A detailed explanation of the γ-activation measurement method used in this study can be found in Refs. [35, 36].

The duration between the end of the irradiation process and beginning of the measurement was between 10 and 15 min, designated as the cooling period. The spectra of each sample were taken many times over a total of 0.5, 1, 12, and 24 h. Fig. 1 and Fig. 2 display the typical γ-ray spectra of the chemical products generated from ^{nat}Cd and ^{nat}Te, respectively. A background spectrum (red line) is also shown in Fig. 1. Bremsstrahlung radiation with an end-point energy of 23 MeV was used to irradiate the samples.

The γ-ray spectra were processed using the DEIMOS32 code [37]. This code uses the Gaussian function to fit the count area of the full-energy peaks. The processed peaks were identified using the half-life of the residual nuclei, γ-ray energy, and intensity. The radionuclides were identified based on their different γ-ray energies and half-lives. Table 2 provides the key γ-ray energies and intensities used to compute the reaction product yield. The columns 4−5 in Table 2 contain the nuclear data from Ref. [38].

The half-lives of previously investigated radionuc-

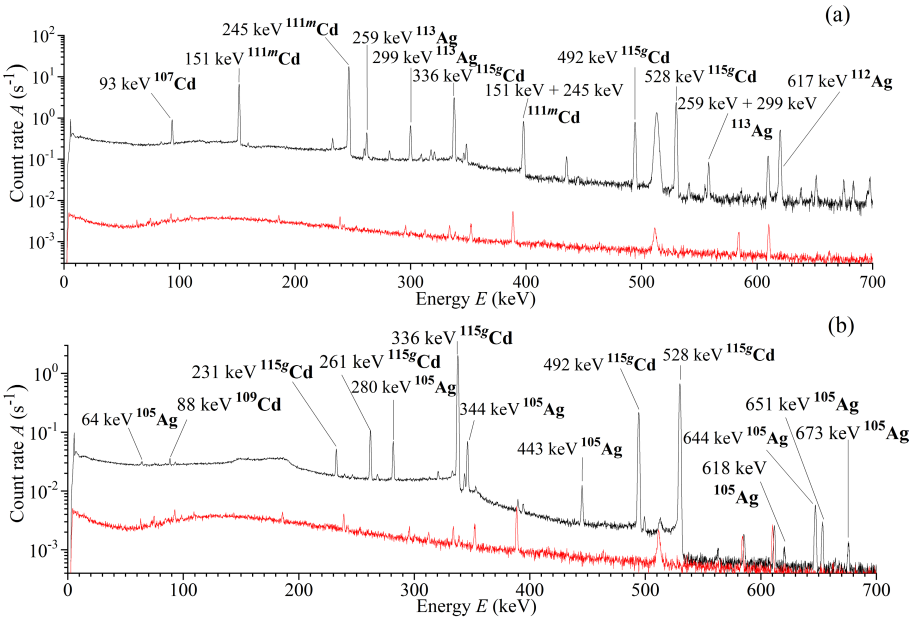

Fig. 1. (color online) Spectra of residual activity of the irradiated sample of ^{nat}Cd (top-to-bottom) 3 h (a) and 4 days (b) after irradiation. The spectra measurement durations were 1 h (a) and 1 day (b), respectively.

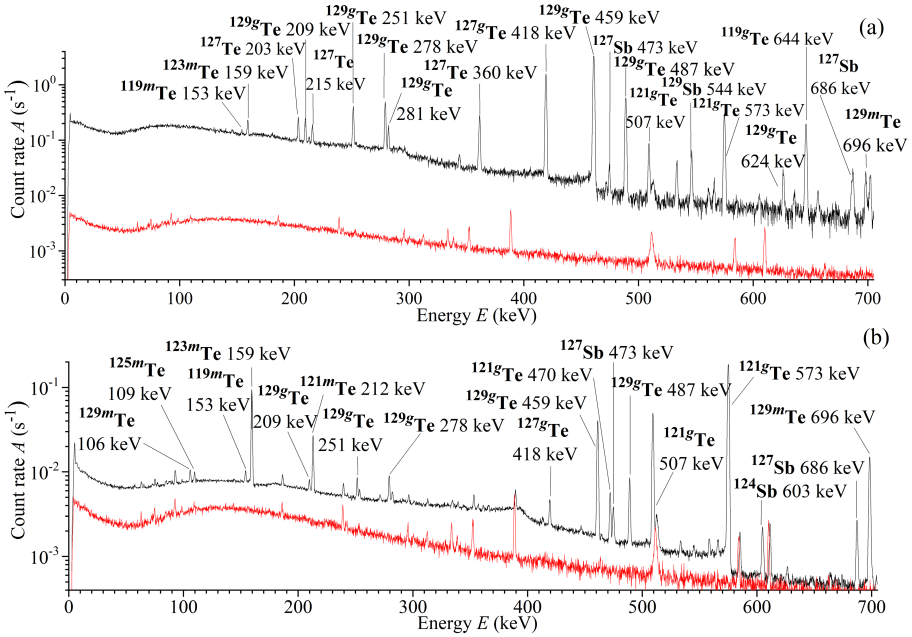

Fig. 2. (color online) Spectra of residual activity of the irradiated sample of ^{nat}Te (top-to-bottom) 6 h (a) and 11 days (b) after irradiation. The spectra measurement durations were 1 h (a) and 3 days (b), respectively.

lides ranged from 20 min (^{115}Ag) to 461.9 days (^{109}Cd) as well as from 69.6 min (^{129g}Te) to 164.2 days (^{121m}Te). To compute the radioactive half-lives and select the appropriate spectra for the activity of each isotope, γ-ray spectra were collected over a range of waiting times, from minutes to a day, after irradiation. The activity is typically measured using the highest intensity, well-separated, interference-free, and correctable γ-ray.

III. DATA ANALYSIS

The experimental yields of the reactions, $Y_{\rm exp}$, were normalized to one electron of the accelerated beam incident on the bremsstrahlung target and calculated using the following formula:

$$Y_{\rm exp} = \frac{S_p \cdot C_{\rm abs}}{\varepsilon \cdot I_\gamma} \frac{t_{\rm real}}{t_{\rm live}} \frac{1}{N} \frac{1}{N_e} \frac{{\rm e}^{\lambda \cdot t_{\rm cool}}}{(1-{\rm e}^{-\lambda \cdot t_{\rm real}})} \frac{\lambda \cdot t_{\rm irr}}{(1-{\rm e}^{-\lambda \cdot t_{\rm irr}})}, \quad (1)$$

where S_p is the full-energy-peak area; ε is the full-energy-peak detector efficiency; I_γ is the γ- emission probability; $C_{\rm abs}$ is the correction for self-absorption of γ-rays in the sample; $t_{\rm real}$ and $t_{\rm live}$ are the real time and live time of the measurement, respectively; N is the number of atoms in the activation sample; N_e is the integral number of incident electrons; λ is the decay constant; $t_{\rm cool}$ is the cooling time; and $t_{\rm irr}$ is the irradiation time.

The experiment determined the yields $Y_{\rm theor}$ of the photonuclear reactions, which reflect the convolution of the photonuclear reaction cross section $\sigma_i(E)$, and distribution density of the number of bremsstrahlung photons over the energy per electron of the accelerator $W(E, E_{\gamma{\rm max}})$. The outcome of measuring the yield of isotope generation in all possible reactions on a natural mixture of isotopes is as follows:

$$Y_{\rm theor}(E_{\gamma{\rm max}}) = \sum_i \eta_i \int_{E_{i{\rm th}}}^{E_{\gamma{\rm max}}} \sigma_i(E)\, W\left(E, E_{\gamma{\rm max}}\right) {\rm d}E, \quad (2)$$

where $E_{\gamma{\rm max}}$ is the kinetic energy of the electrons hitting the tungsten radiator, E is the energy of bremsstrahlung photons produced on the radiator, $E_{\rm th}$ is the threshold of the studied photonuclear reaction, η_i is the percentage of the studied isotope in the natural mixture, and the index i corresponds to the number of reactions contributing to the production of the studied isotope.

Figure 3 illustrates the distribution density of the number of bremsstrahlung photons $W(E, E_{\gamma{\rm max}})$ per electron of the accelerator for accelerated electron energies from 10 to 23 MeV, determined using Geant4 for the bremsstrahlung target made of tungsten with a thickness of 3 mm.

The total and partial cross sections $\sigma(E)$ of the photonuclear reactions on the cadmium and tellurium isotopes were estimated for monochromatic photons using the TALYS code [24] with standard parameters and CMPR [25]. The TALYS program examines all processes in the nucleus and transitions between the states. As a result, it is possible to calculate not only the total cross section of a photonuclear reaction but also the cross sections of reactions involving the production of certain states, particu-

Table 2. Spectroscopic data from Ref. [38] for the product nuclei from the photonuclear reactions on stable isotopes of cadmium and tellurium.

Nucleus	Half-life $T_{1/2}$	Decay mode (%)	γ-ray energy E_γ/keV (I_γ (%))	Reaction	E_{th}/MeV
Data for irradiated cadmium target					
^{105}Cd	55.5 m	EC	346.87 (4.2), 961.84 (4.69)	^{106}Cd(γ, *n*)	10.9
^{107}Cd	6.5 h	EC	93.124 (4.7)	^{108}Cd(γ, *n*)	10.3
^{109}Cd	461.9 d	EC	88.03 (3.644)	^{110}Cd(γ, *n*)+ ^{111}Cd(γ, 2*n*)	9.9 16.89
^{111m}Cd	48.54 m	IT	150.82 (29.1), 245.39 (94)	^{112}Cd(γ, *n*)+ ^{113}Cd(γ, 2*n*)	9.4 15.93
^{115g}Cd	53.46 h	β$^-$	336.24 (46.02), 527.9 (27.45)	^{116}Cd(γ, *n*)	8.7
^{115m}Cd	44.56 d	β$^-$	933.8 (2)	^{116}Cd(γ, *n*)	8.9
^{105}Ag	41.29 d	EC	280.41 (30.2), 344.52 (41)	^{106}Cd(γ, *p*)	7.4
^{111}Ag	7.45 d	β$^-$	342.13 (6.7)	^{112}Cd(γ, *p*)+ ^{113}Cd(γ, *np*)	9.6 16.19
^{112}Ag	3.13 h	β$^-$	617.51 (43), 1387.68 (5.3)	^{113}Cd(γ, *p*)+ ^{114}Cd(γ, *np*)	9.7 18.76
^{113}Ag	5.37 h	β$^-$	298.6 (10)	^{114}Cd(γ, *p*)	10.3
^{115}Ag	20 m	β$^-$	229.1 (18)	^{116}Cd(γ, *p*)	11
Data for irradiated tellurium target					
^{119g}Te	16.05 h	EC	644.01 (84.1), 699.85 (10.1)	^{120}Te(γ, *n*)	10.29
^{119m}Te	4.7 d	EC	153.59 (66), 1212.73 (66.1)	^{120}Te(γ, *n*)	10.55
^{121g}Te	19.17 d	EC	573.14 (80.4)	^{122}Te(γ, *n*)+ ^{123}Te(γ, 2*n*)	9.83 16.76
^{121m}Te	164.2 d	IT: 88.6 EC: 11.4	212.19 (81.5)	^{122}Te(γ, *n*)+ ^{123}Te(γ, 2*n*)	10.12 17.05
^{123m}Te	119.2 d	IT	159.0 (84.3)	^{123}Te(γ, γ`)+ ^{124}Te(γ, *n*)+ ^{125}Te(γ, 2*n*)	 9.67 16.24
^{125m}Te	57.4 d	IT	109.28 (0.28)	^{125}Te(γ, γ`)+ ^{126}Te(γ, *n*)	 9.25
^{127}Te	9.35 h	β$^-$	417.9 (0.99)	^{128}Te(γ, *n*)	8.78
^{129g}Te	69.6 min	β$^-$	459.60 (7.7)	^{130}Te(γ, *n*)	8.42
^{129m}Te	33.6 d	IT: 64 EC: 36	695.88 (3.0)	^{130}Te(γ, *n*)	8.52
^{122}Sb	2.72 d	β$^-$:97.59 EC: 2.41	564.24 (70.67)	^{123}Te(γ, *p*)+ ^{124}Te(γ, *np*)	8.13 17.55
^{124}Sb	60.2 d	β$^-$	602.72 (97.8), 1690.97 (47.57)	^{125}Te(γ, *p*)+ ^{126}Te(γ, *np*)	8.69 17.80
^{127}Sb	3.85 d	β$^-$	473.0 (25.8), 685.7 (36.8)	^{128}Te(γ, *p*)	9.58
^{129}Sb	4.366 h	β$^-$	812.97 (48.2), 914.96 (23.3)	^{130}Te(γ, *p*)	10.01

larly isomeric states. The standard (default) TALYS option uses the Simple Modified Lorentzian (SMLO) model for photon strength functions (PSFs). This model is used to calculate *E*1, *M*1, and upbend components, generally providing more accurate, temperature-dependent resonance shapes than those achieved with older models.

When compared with TALYS, the CMPR accurately considers the GDR isospin splitting, which is crucial for describing the proton decay channel. The basics of the GDR isospin splitting and some relevant CMPR results are presented in Appendix B. This Appendix also provides information on TALYS options as well as examples of comparison between the TALYS and CMPR results.

The yield measurement for a natural mixture of isotopes yields gives the amount of isotope produced in all potential reactions on the natural mixture. The primary problem of bremsstrahlung beam experiments is that the

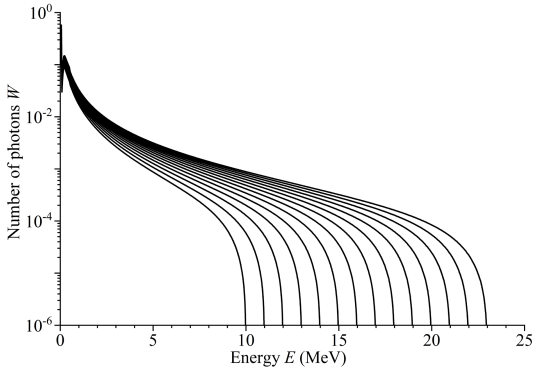

Fig. 3. Distribution density of the number of bremsstrahlung photons at the energies of 10−23 MeV

yield of photonuclear reaction depends on both the investigated cross section of the reaction $\sigma_i(E)$ and the form of the bremsstrahlung spectrum $W(E, E_{\gamma\max})$, which is often known with inadequate accuracy. The use of relative yields allows us to determine the dependency of the yield of photonuclear reactions on the maximal energy of bremsstrahlung under various experimental settings. The overall photon absorption cross section is not taken into account when calibrating the yield of one of the most likely reactions. The the most probable and well-studied ^{116}Cd(γ, n)^{115}Cd and ^{130}Te(γ, n)^{129}Te reactions were chosen as a primary reaction in case of cadmium and tellurium, respectively. In addition, there are no other channels (for example, (γ, 2n) reaction on heavier stable nuclei) for the product formation of ^{115}Cd and ^{129}Te, as the nuclei ^{116}Cd and ^{130}Te are the heaviest stable nuclei in the natural mixture of Cd and Te.

The theoretical values of the relative yields can be calculated using the following formula:

$$Y_{\rm rel}(E_{\gamma\max}) = \frac{\sum_i \eta_i \int_{E_{\rm th}}^{E_{\gamma\max}} \sigma_i(E)\, W\left(E, E_{\gamma\max}\right) {\rm d}E}{\eta \int_{E_{\rm th}}^{E_{\gamma\max}} \sigma_{(\gamma,n)}(E)\, W\left(E, E_{\gamma\max}\right) {\rm d}E}, \quad (3)$$

where η denotes the percentages of the ^{116}Cd and ^{130}Te isotopes in the natural mixture of cadmium and tellurium isotopes, respectively. Owing to the assumption regarding the unchanged shape of the bremsstrahlung spectrum, the bremsstrahlung spectrum $W(E, E_{\gamma\max})$ can be replaced by the photon production cross section $\sigma(E, E_{\gamma\max})$ calculated using the Seltzer-Berger tables [39].

$$Y_{\rm rel}(E_{\gamma\max}) = \frac{\sum_i \eta_i \int_{E_{\rm th}}^{E_{\gamma\max}} \sigma_i(E)\sigma\left(E, E_{\gamma\max}\right) {\rm d}E}{\eta \int_{E_{\rm th}}^{E_{\gamma\max}} \sigma_{(\gamma,n)}(E)\sigma\left(E, E_{\gamma\max}\right) {\rm d}E}. \quad (4)$$

To represent the experimental photonuclear reaction data, the cross section per equivalent quantum σ_q, determined by the following expression, is used:

$$\sigma_q(E_{\gamma\max}) = \frac{\int_{E_{\rm th}}^{E_{\gamma\max}} \sigma(E)\sigma\left(E, E_{\gamma\max}\right) {\rm d}E}{\frac{1}{E_{\gamma\max}} \int_0^{E_{\gamma\max}} E\cdot\sigma\left(E, E_{\gamma\max}\right) {\rm d}E}. \quad (5)$$

The cross section per equivalent quantum for a natural mixture of isotopes includes all possible channels of the final isotope production, where the percentage of initial nuclei is accounted for as follows:

$$\sigma_q^{\rm nat}(E_{\gamma\max}) = \frac{\sum_{i=1}^{8} \eta_i \int_{E_{\rm th}}^{E_{\gamma\max}} \sigma_i(E)\sigma\left(E, E_{\gamma\max}\right) {\rm d}E}{\frac{1}{E_{\gamma\max}} \int_0^{E_{\gamma\max}} E\cdot\sigma\left(E, E_{\gamma\max}\right) {\rm d}E}. \quad (6)$$

The experimental points along the cross sections of the (γ, n) [22] and (γ, n) + (γ, pn) [16] reactions on the isotopes ^{120,128,130}Te were approximated by the Lorentz function, and the relative yields $Y_{\rm rel}$ and cross sections per equivalent quantum σ_q were calculated based on the least squares approximation. In Figs. 4−10, these points are indicated by open circles [22] and open rectangles [16], respectively.

IV. RESULTS AND DISCUSSION

The measured yields relative to the yield of the reaction ^{116}Cd(γ, n)^{115}Cd (in the case of $^{\rm nat}$Cd) and ^{130}Te(γ, n)^{129}Te (in the case of $^{\rm nat}$Te) and cross sections per equivalent quantum for a natural mixture of isotopes are shown in Figs. 4−25 and Tables A1−A2 in Appendix A, along with theoretical computations using the TALYS and CMPR programs and previously published data.

The square root of the quadratic sum of all independent statistical and systematic uncertainties was used to determine the overall uncertainties in the results. The counting statistics from the observed number of counts under the photo-peak of each γ-line (2.5%−10.5%) were the primary contributors to the ensuing statistical uncertainty. Data accumulation for an optimal duration of measurements based on the half-life of the generated nuclides was used to estimate this. In addition, the systematic uncertainties were computed using the uncertainties in the following: number of target nuclei (~0.3%), irradiation and cooling time (~0.5%), current and electron beam energy (~2.5%), detector efficiency (~3%), half-life of reaction products (~2%), distance between the sample and detector (~2%), γ-ray abundance (~2%), flux estimation (~11.5%), and normalization of the experimental data to

the yield of the ^{116}Cd(γ, n)^{115}Cd and ^{130}Te(γ, n)^{129}Te monitor reactions (0.5%−2%). The overall systematic uncertainty is approximately 12.58%. It is determined that the overall uncertainty ranges from approximately 12% to approximately 19%.

A. Photonuclear reactions on cadmium isotopes

1. *Photoneutron reactions*

Five cadmium isotopes are directly generated by ^{nat}Cd(γ, n) reactions when natural cadmium is irradiated with bremsstrahlung radiation with an end-point energy of 10−23 MeV. In this study, the relative yields and cross section per equivalent quantum of the ^{nat}Cd(γ, n)^{105,107,109,111m,115g,115m}Cd reactions at the bremsstrahlung end-point energies of 10−23 MeV were determined, and the results are presented in Figs. 4−8. In addition, the tabulated results are given in Appendix A.

(a) ^{106}Cd(γ, n)^{105}Cd reaction

No literature data are available for this reaction; hence, its measurements were compared only with the theoretical calculations. Figure 4 shows the experimentally obtained and simulated values of the relative yield as well as cross section per equivalent quantum of the reaction ^{106}Cd(γ, n)^{105}Cd. In Fig. 4, it is clear that the cross section per equivalent quantum, calculated by the TALYS and CMPR codes, are almost the same, but they are higher than the currently presented results for the ^{106}Cd(γ, n)^{105}Cd reaction.

At an energy of 12 MeV, the theoretical values for the two models are 4 times higher than the experimental values. When the energy is increased to 20 MeV, the ratio $\sigma^{nat}_{q\exp}/\sigma^{nat}_{q\text{theory}}$ decreases and is equal to approximately 2.5. The apparent disparity between the theoretical and experimental values may stem from the fact that statistical models of photonuclear reactions, such as the CMPR and TALYS codes, overlook the unique structural characteristics of cadmium isotopes. Alternatively, the low experimental neutron yield in the reaction ^{106}Cd(γ, n)^{105}Cd can be partly explained by the bypassed character of the nucleus ^{106}Cd.

(b) ^{108}Cd(γ, n)^{107}Cd reaction

Figure 5 shows that the current results follow the graphical shape but are lower than the theoretical values. The experimental results (γ, n) are two times lesser than

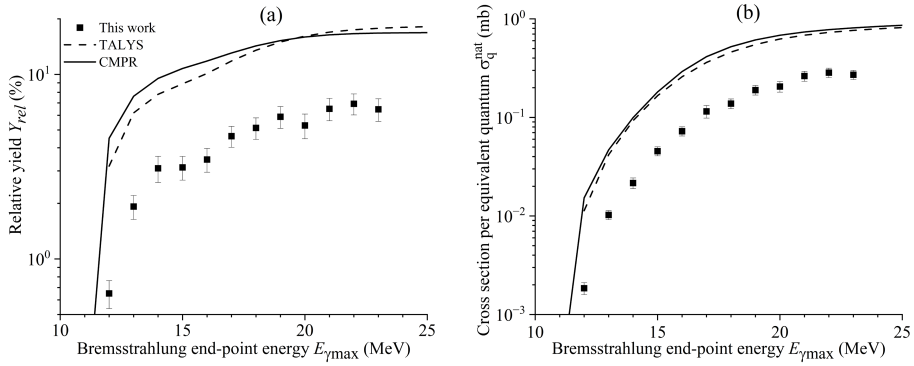

Fig. 4. Relative yields (a) and cross section per equivalent quantum (b) of reaction ^{106}Cd(γ, n)^{105}Cd as functions of the bremsstrahlung end-point energy from this study (solid rectangles) and simulated values using the CMPR (solid lines) and TALYS code (dashed lines).

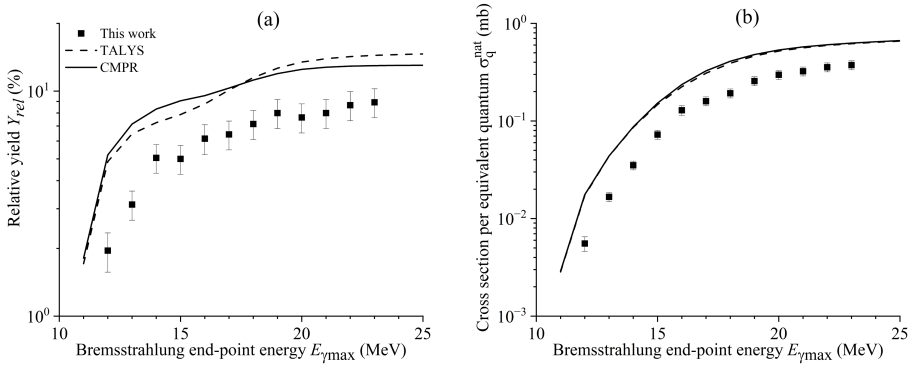

Fig. 5. Relative yields (a) and cross section per equivalent quantum (b) of reaction ^{108}Cd(γ, n)^{107}Cd as functions of the bremsstrahlung end-point energy from this study (solid rectangles) as well as simulated values using the CMPR (solid lines) and TALYS code (dashed lines).

the corresponding theoretical values. This discrepancy indicates the need for further research on photoneutron reactions on ^{106,108}Cd.

(c) ^{110}Cd(γ, n)^{109}Cd and ^{111}Cd(γ, 2n)^{109}Cd reactions

Regarding the production of ^{109}Cd from the ^{nat}Cd(γ, Xn)^{109}Cd reactions, only one previous experimental data set in the GDR energy region based on the bremsstrahlung photons is available [3]; the values were found to be lower than the theoretical values obtained using the TALYS and CMPR codes, as shown in Fig. 6. The figure shows that the current results follow the graphical shape but are lower than the theoretical values; they are the closest to the values calculated using the TALYS code.

(d) ^{111}Cd(γ, γ`)^{111m}Cd and ^{112}Cd(γ, n)^{111m}Cd reactions

The measured results for the ^{111}Cd(γ, γ`)^{111m}Cd and ^{112}Cd(γ, n)^{111m}Cd reactions are compared with the theoretical values obtained with the TALYS and CMPR codes in Fig. 7. For the production of ^{111m}Cd from the ^{nat}Cd target, only one previous experimental data set in the GDR energy region based on bremsstrahlung photons is available [3]. The value was found to be lower than the theoretical values obtained using the TALYS code, as shown in Fig. 7. The figure also shows that the theoretical values from both the TALYS and CMPR codes as well as literature data are in agreement with the data from this study. Based on Fig. 7, it can also be said that in the energy range up to 11 MeV, the ^{111m}Cd nucleus is formed by the ^{111}Cd(γ, γ`)$^{111m}$Cd reaction, and the contributions of the $^{111}$Cd(γ, γ`)^{111m}Cd and ^{112}Cd(γ, n)^{111m}Cd reactions to the formation of ^{111m}Cd are equal at 12 MeV, after which the ^{112}Cd(γ, n)^{111m}Cd reaction plays the dominant role.

(e) ^{116}Cd(γ, n)^{115m,g}Cd reaction

The measured results for the ^{116}Cd(γ, n)^{115m,g}Cd reactions are compared with the theoretical values obtained using the TALYS and CMPR codes in Fig. 8. Only one value is available in literature for the ^{116}Cd(γ, n)^{115m,g}Cd reaction [3] at 23 MeV. As shown in Fig. 8, it is clear that the theoretical values from both the TALYS and CMPR codes as well as the literature value are in agreement with the data from this study.

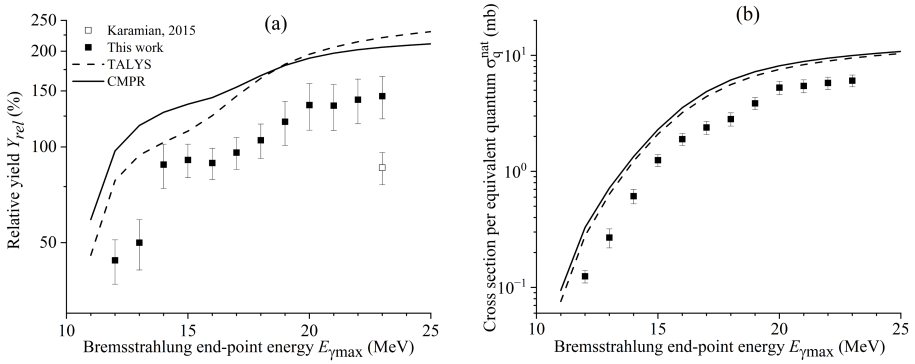

Fig. 6. Relative yields (a) and cross section per equivalent quantum (b) of reactions ^{110}Cd(γ, n)^{109}Cd and ^{111}Cd(γ, 2n)^{109}Cd as functions of the bremsstrahlung end-point energy from this study (solid rectangles), literature data [3] (open rectangle), and simulated values using the CMPR (solid lines) and TALYS code (dashed lines).

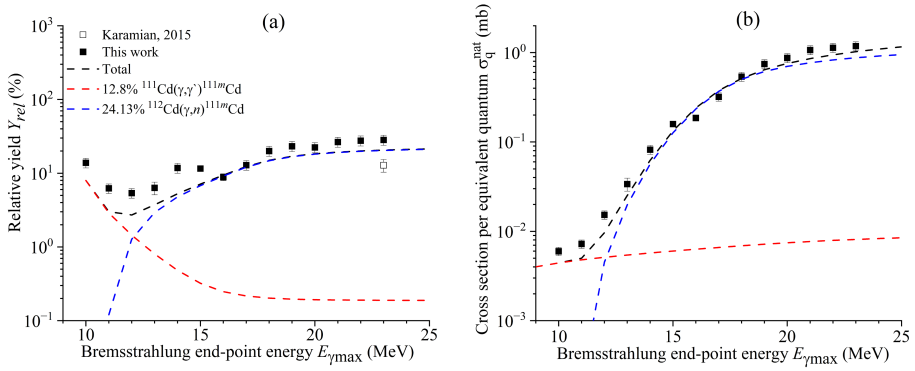

Fig. 7. (color online) Relative yields (a) and cross section per equivalent quantum (b) of ^{111}Cd(γ, γ`)^{111m}Cd and ^{112}Cd(γ, n)^{111m}Cd reactions as functions of bremsstrahlung end-point energy from this study (solid rectangles), literature data [3] (open rectangle), and simulated values using TALYS code (dashed lines).

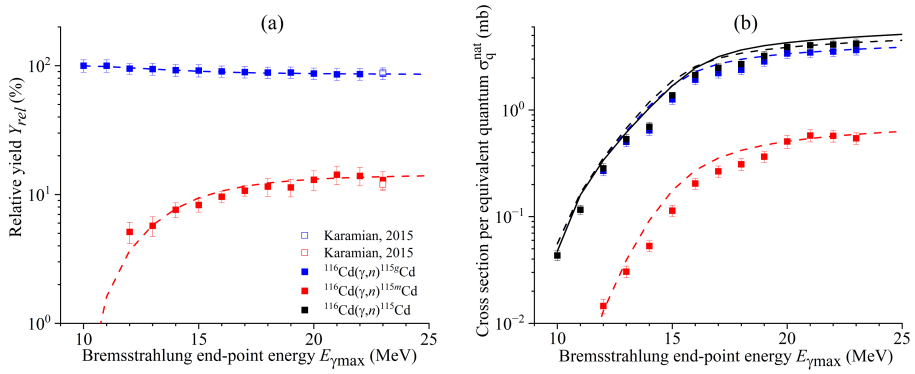

Fig. 8. (color online) Relative yields (a) and cross section per equivalent quantum (b) of reaction ^{116}Cd(γ, n)^{115}Cd as functions of bremsstrahlung end-point energy from this study (solid rectangles), literature data [3] (open rectangles), and simulated values using the CMPR (solid line) and TALYS code (dashed lines).

2. *Photoproton reactions*

Five argentum isotopes are directly generated by the ^{nat}Cd(γ, p) reactions when natural cadmium is irradiated with bremsstrahlung radiation with the end-point energy of 10−23 MeV. The relative yields and cross section per equivalent quantum of the ^{nat}Cd(γ, p)^{105,111,112,113,115}Ag reactions at the bremsstrahlung end-point energies of 12−23 MeV were determined for the first time in this study, and the results are presented in Figs. 9−14.

(a) ^{106}Cd(γ, p)^{105}Ag reaction

These measurements were compared only with the theoretical values owing to unavailability of published data. In Fig. 9, the measured values are revealed to be higher than the calculated values. No theoretical calculation can describe the experimental data.

The ratio $\sigma^{nat}_{qexp}/\sigma^{nat}_{qtheory}$ is approximately 10 for the two models. As discussed in Section A1, the proton Fermi surface is significantly higher than the neutron Fermi surface in the ^{106}Cd nucleus. Because of a reduction in the effective width of the Coulomb barrier, this must raise the proton penetrabilities and, consequently, the proton yield.

The proton yield on ^{106}Cd can also be boosted by the direct photoelectric effect, which is predominantly localized at the nucleus surface. Protons are expected to dominate in β$^+$-radioactive nuclei and the nuclei bordering them. The structural (shell) unique features of the target nucleus have a significant effect on the direct photonuclear reactions. Cadmium isotopes exhibit the most significant single-particle dipole excitations during the $1g_{9/2} \rightarrow 1h_{11/2}$ transitions. The decay of such excitations, which have a probability of approximately 40% in both the proton and neutron channels, leads to the emission of protons with the maximum possible energy, because the final-state nucleus {Z–1, N} arises in the ground state. The energy carried away by neutrons is 3 to 4 MeV smaller, because the final-state nucleus {Z, N–1} remains in an excited (hole) state. This significantly influences the relative output of protons and neutrons in proton-rich cadmium isotopes.

Figure 10 shows the relative yields of ^{106}Cd(γ, n)^{105}Cd and ^{106}Cd(γ, p)^{105}Ag reactions as well as the sum of the values for the ^{106}Cd(γ, n)^{105}Cd and ^{106}Cd(γ, p)^{105}Ag reactions. The results in Fig. 10 show that the theoretical yields of the (γ, n) and (γ, p) reactions on ^{106}Cd nuclei differ significantly from their experimental counterparts, but their summed value agrees with the respective experi-

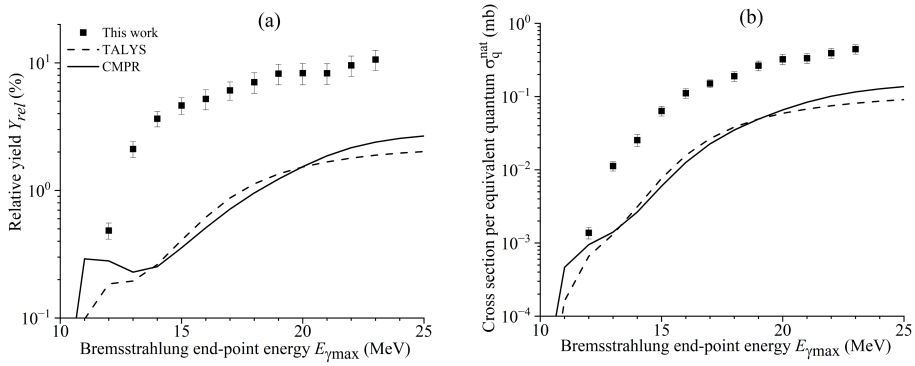

Fig. 9. Relative yields (a) and cross section per equivalent quantum (b) of reaction ^{106}Cd(γ, p)^{105}Ag as functions of bremsstrahlung end-point energy from this study (solid rectangles) and simulated values using the CMPR (solid lines) and TALYS code (dashed lines).

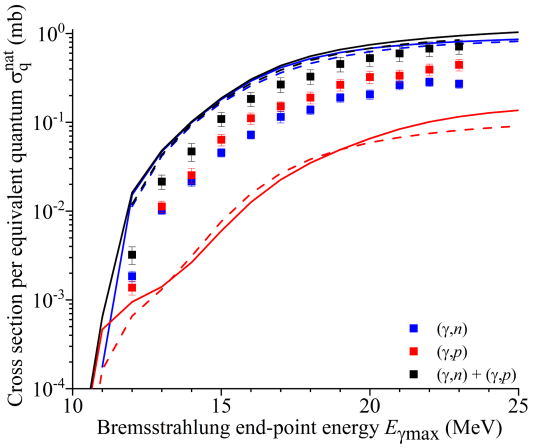

Fig. 10. (color online) Cross section per equivalent quantum of ^{106}Cd(γ, *n*)^{105}Cd and ^{106}Cd(γ, *p*)^{105}Ag reactions as functions of the bremsstrahlung end-point energy from this study (solid rectangles) and simulated values using the CMPR (solid lines) and TALYS code (dashed lines).

mental value. This means that the original photoabsorption cross section calculated using the TALYS code is unlikely to differ significantly from the true value. The discrepancy in the cross section per equivalent quantum is owing to the redistribution of the cross section between the (γ, *n*) and (γ, *p*) reactions.

(b) ^{112}Cd(γ, *p*)^{111}Ag reaction

For the ^{112}Cd(γ, *p*)^{111}Ag reaction only one previous experimental data sets in 23 MeV [3]; this was found to be lower than the theoretical values obtained using the CMPR code as shown in Fig. 11. In Fig. 11, it is shown that the currently measured and theoretical values based on the CMPR code are in good agreement, in terms of not only shape but also magnitude. TALYS predicts results that are approximately 5 times lower than CMPR, and this difference increases rapidly with increasing energy.

(c) ^{113}Cd(γ, *p*)^{112}Ag reaction

For the ^{113}Cd(γ, *p*)^{112}Ag reaction only one previous experimental data sets in 23 MeV [3]; this was found to be lower than the theoretical values obtained using the CMPR code as shown in Fig. 12. In Fig. 12, the measured values for the reaction are higher than the calculated values; however, they are the closest to the values calculated using the CMPR code. TALYS predicts results that

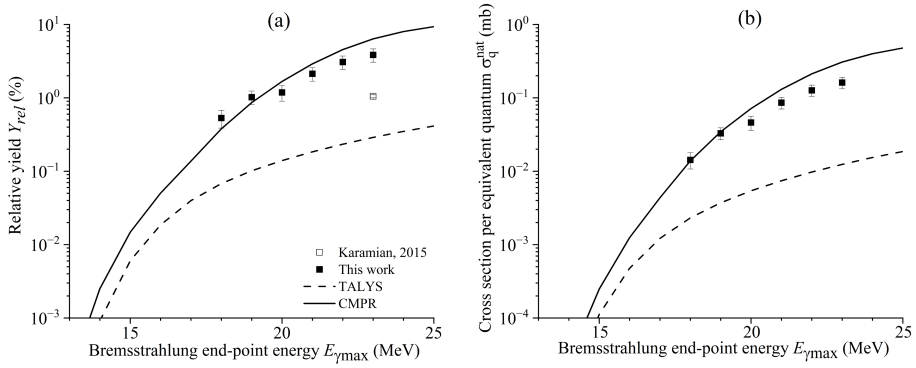

Fig. 11. Relative yields (a) and cross section per equivalent quantum (b) of reaction ^{112}Cd(γ, *p*)^{111}Ag as functions of the bremsstrahlung end-point energy from this study (solid rectangles), literature data [3] (open rectangle), and simulated values using the CMPR (solid lines) and TALYS code (dashed lines).

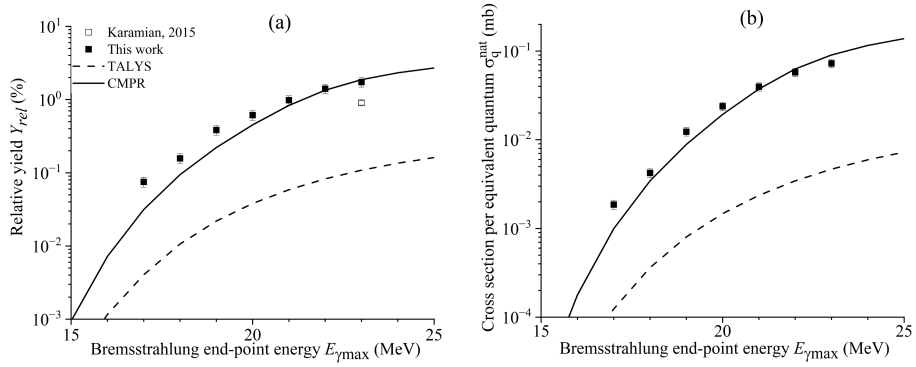

Fig. 12. Relative yields (a) and cross section per equivalent quantum (b) of reaction ^{113}Cd(γ, *p*)^{112}Ag as functions of the bremsstrahlung end-point energy from this study (solid rectangles), literature data [3] (open rectangle), and simulated values using the CMPR (solid lines) and TALYS code (dashed lines).

are approximately 5 times lower than CMPR, and this difference increases rapidly with increasing energy.

(d) ^{114}Cd(γ, p)^{113}Ag reaction

For the ^{114}Cd(γ, p)^{113}Ag reaction, only one previous experimental data set is available for 23 MeV [3]; this value was found to be lower than the theoretical values obtained using the CMPR code, as shown in Fig. 13. In Fig. 13, the measured values for the reaction are higher than the calculated values; however, they are the closest to the values calculated using the CMPR code. The results predicted by TALYS are approximately 5 times lower than the CMPR values, and this difference increases rapidly with increasing energy.

As can be seen in Figs. 11−13, a discrepancy in the experimental data for the reactions ^{nat}Cd(γ, p)$^{111\text{-}113}$Ag is clearly observed, where our results are higher than the literature data [3]. The large difference between the results in [3] and those of this study for the reactions ^{nat}Cd(γ, p)$^{111\text{-}113}$Ag might have originated from the difference in the measurement duration of the irradiated targets.

(e) ^{116}Cd(γ, p)^{115}Ag reaction

The measurements from the reaction were compared with only the theoretical values owing to unavailability of published data. In Fig. 14, the measured values for the reaction are higher than the calculated values; however, they are the closest to the values calculated using the CMPR code. The results predicted by TALYS are approximately 16 times lower than the CMPR results.

B. Photonuclear reactions on tellurium isotopes

1. *Photoneutron reactions*

Nine tellurium isotopes are directly generated by the ^{nat}Te(γ, n) reactions when natural tellurium is irradiated with bremsstrahlung radiation with an end-point energy of 10-23 MeV. In this study, the relative yields and cross sections per equivalent quantum of the ^{nat}Te(γ, n)^{119g,119m,121g,121m,123m,125m,127,129g,129m}Te reactions at the bremsstrahlung end-point energies of 10−23 MeV were determined, and the results are presented in Figs. 15−20.

(a) ^{120}Te(γ, n)^{119}Te reaction

The measured results for the ^{120}Te(γ, n)^{119m,g}Te reactions are compared with the theoretical values obtained with the TALYS and CMPR codes in Fig. 15. There is only one value in literature for the ^{120}Te(γ, n)^{119}Te reaction [22] in the energy range of the γ quantum

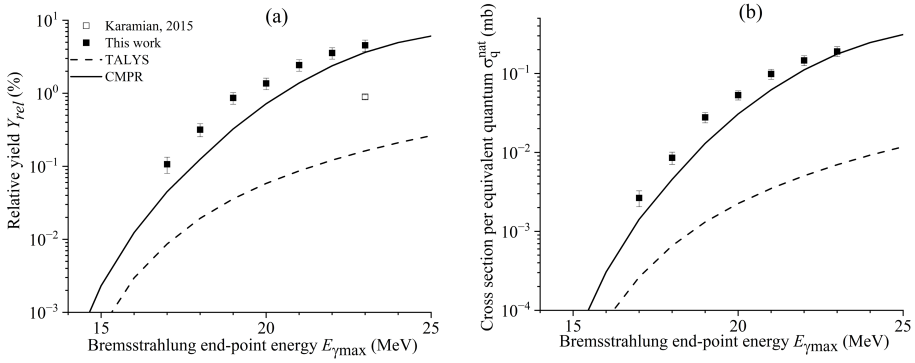

Fig. 13. Relative yields (a) and cross section per equivalent quantum (b) of reaction ^{114}Cd(γ, p)^{113}Ag as functions of the bremsstrahlung end-point energy from this study (solid rectangles), literature data [3] (open rectangle), and simulated values using the CMPR (solid lines) and TALYS code (dashed lines).

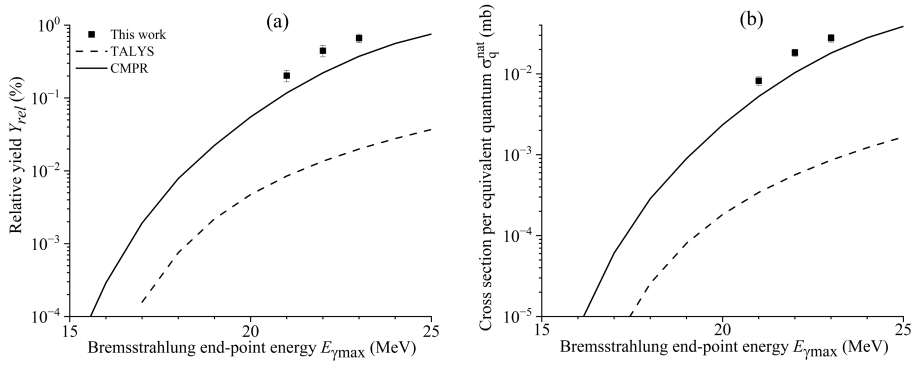

Fig. 14. Relative yields (a) and cross section per equivalent quantum (b) of reaction ^{116}Cd(γ, p)^{115}Ag as functions of bremsstrahlung end-point energy from this study (solid rectangles) and simulated values using the CMPR (solid lines) and TALYS code (dashed lines).

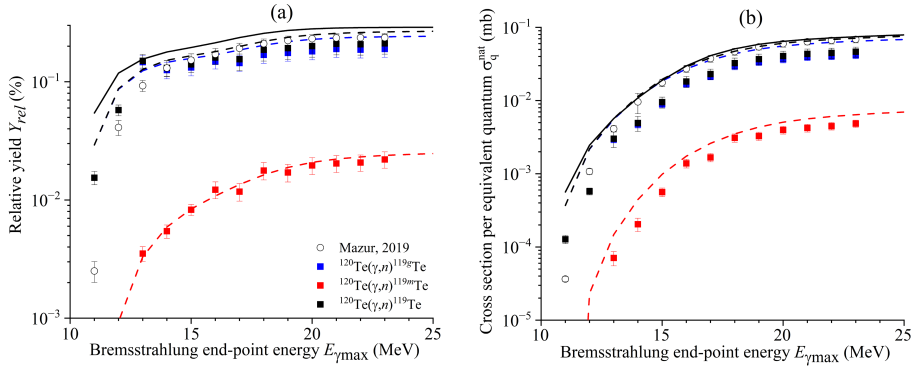

Fig. 15. (color online) Relative yields (a) and cross section per equivalent quantum (b) of reaction ^{120}Te(γ, n)^{119}Te as functions of the bremsstrahlung end-point energy from this study (solid rectangles), literature data [22] (open circles), and simulated values using the CMPR (solid lines) and TALYS code (dashed lines).

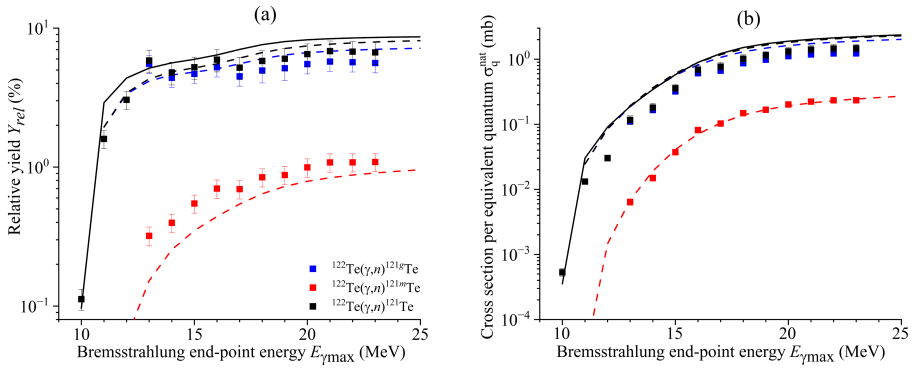

Fig. 16. (color online) Relative yields (a) and cross section per equivalent quantum (b) of the ^{122}Te(γ, n)^{121}Te and ^{123}Te(γ, 2n)^{121}Te reactions as functions of the bremsstrahlung end-point energy from this study (solid rectangles) and simulated values using the CMPR (solid lines) and TALYS code (dashed lines).

(8.03−26.46 MeV). The theoretical values from both the TALYS and CMPR codes align with the literature data; however, our results are inferior to them, as shown in Fig. 15.

(b) ^{122}Te(γ, n)^{121}Te and ^{123}Te(γ, 2n)^{121}Te reactions

The measured results for the ^{122}Te(γ, n)^{121}Te and ^{123}Te(γ, 2n)^{121}Te reactions are compared with the theoretical values obtained with the TALYS and CMPR codes in Fig. 16. The figure shows that the measured values for the reaction are lower than the calculated values.

(c) ^{123}Te(γ, γ`)^{123m}Te, ^{124}Te(γ, n)^{123m}Te and ^{125}Te(γ, 2n)^{123m}Te reactions

The measured results for the ^{123}Te(γ, γ`)^{123m}Te, ^{124}Te(γ, n)^{123m}Te, and ^{125}Te(γ, 2n)^{123m}Te reactions are compared with the theoretical values obtained with the TALYS code in Fig. 17. The figure shows that the measured values for the reaction are lower than the calculated values.

(d) ^{125}Te(γ, γ`)^{125m}Te and ^{126}Te(γ, n)^{125m}Te reactions

The measured results for the ^{125}Te(γ, γ`)^{125m}Te and ^{126}Te(γ, n)^{125m}Te reactions are compared with the theoretical values obtained with the TALYS code in Fig. 18. As can be seen in Fig. 18(a), the measured values for the reaction are higher than the calculated values. This may be because the nucleus ^{125m}Te emits a γ-ray with a low intensity (109.28 keV (0.28%)). However, with the exception of the data for 10−12 MeV, a good agreement is observed between the measured data and TALYS value in Fig. 18(b).

(e) ^{128}Te(γ, n)^{127}Te reaction

The measured results for the ^{128}Te(γ,n)^{127}Te reaction are compared with the theoretical values obtained with TALYS in Fig. 19. The figure shows that the measured values for the reaction are lower than the calculated values. There is a good agreement between the literature data and theoretical calculations.

(f) ^{130}Te(γ, n)^{129}Te reaction

The measured results for the ^{120}Te(γ, n)^{119m,g}Te reactions are compared with the theoretical values obtained with the TALYS and CMPR codes in Fig. 20. Only one value is available in literature for the ^{130}Te(γ, n)^{129}Te reaction [22] in the energy range of the γ quantum (8.03−26.46 MeV). It is clear that the theoretical values from both the

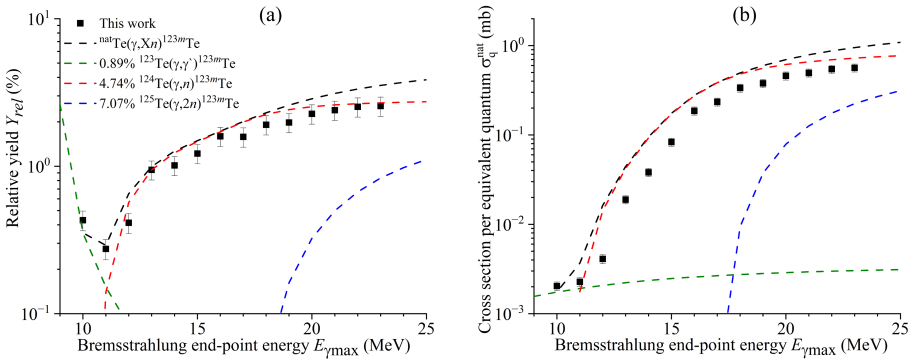

Fig. 17. (color online) Relative yields (a) and cross section per equivalent quantum (b) of ^{123}Te(γ, γ`)^{123m}Te, ^{124}Te(γ, n)^{123m}Te, and ^{125}Te(γ, 2n)^{123m}Te reactions as functions of the bremsstrahlung end-point energy from this study (solid rectangles) and simulated values using TALYS code.

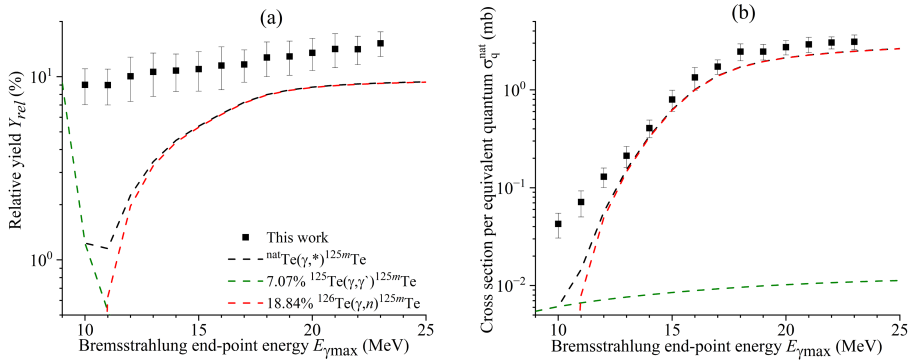

Fig. 18. (color online) Relative yields (a) and cross section per equivalent quantum (b) of ^{125}Te(γ, γ`)^{125m}Te and ^{126}Te(γ, n)^{125m}Te reactions as functions of the bremsstrahlung end-point energy from this study (solid rectangles) and simulated values using TALYS code.

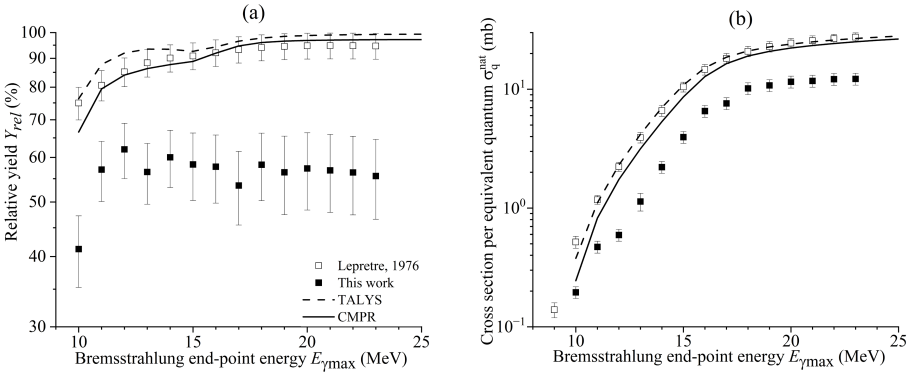

Fig. 19. Relative yields (a) and cross section per equivalent quantum (b) of ^{128}Te(γ, n)^{127}Te reaction as functions of the bremsstrahlung end-point energy from this study (solid rectangles), literature data [22] (open rectangles), and simulated values using the CMPR (solid lines) and TALYS code (dashed lines).

TALYS and CMPR codes are in agreement with the literature data, but our results are lower, as shown in Fig. 20.

2. *Photoproton reactions*

Four stibium (^{122}Sb, ^{124}Sb, ^{127}Sb, ^{129}Sb) radioisotopes were directly produced by the ^{nat}Te(γ, p) reactions. The relative yields and cross section per equivalent quantum of the ^{nat}Te(γ, p)^{122,124,127,129}Sb reactions at the bremsstrahlung end-point energies of 10−23 MeV were determined for the first time in this study and are presented in Figs. 21−25.

(a) ^{123}Te(γ, p)^{122}Sb and ^{124}Te(γ, np)^{122}Sb reactions

Figure 21 displays the measured data and computed values. It is evident from Fig. 21 that the theoretical values based on the CMPR show a good agreement only for 22 and 23 MeV. The remaining experimental points are

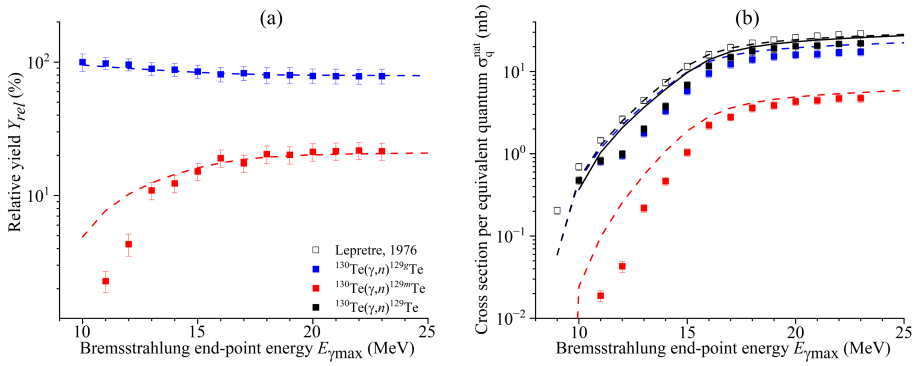

Fig. 20. (color online) Relative yields (a) and cross section per equivalent quantum (b) of the reaction ^{130}Te(γ, n)^{129}Te as functions of the bremsstrahlung end-point energy from this study (solid rectangles), literature data [22] (open rectangles), and simulated values using the CMPR (solid line) and TALYS code (dashed lines).

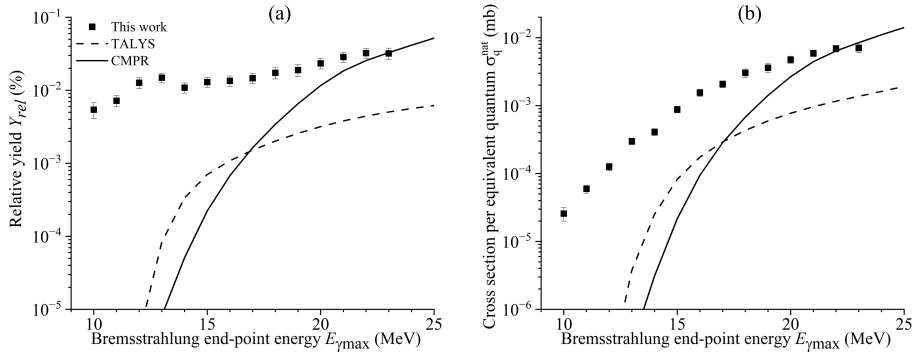

Fig. 21. Relative yields (a) and cross section per equivalent quantum (b) of the ^{123}Te(γ, p)^{122}Sb and ^{124}Te(γ, np)^{122}Sb reactions as functions of the bremsstrahlung end-point energy from this study (solid rectangles) and simulated values using the CMPR (solid lines) and TALYS code (dashed lines).

almost 100 times larger than the theoretical calculations.

Because the threshold of the reaction ^{124}Te(γ, d)^{122}Sb is 15.33 MeV, we can assume that up to 19 MeV (considering the Coulomb barrier), the nucleus ^{122}Sb is formed as a result of the reaction ^{123}Te(γ, p). Figure 22 shows the ratios of the cross section per equivalent quantum $\sigma^{nat}_{qexp}/\sigma^{nat}_{qtheory}$ for the (γ, p) reaction on ^{123}Te. As can be seen in Fig. 22, both models cannot describe the experimental points.

(b) ^{125}Te(γ, p)^{124}Sb and ^{126}Te(γ, np)^{124}Sb reactions

The measured results for the ^{125}Te(γ, p)^{124}Sb and ^{126}Te(γ, np)^{124}Sb reactions are compared with the theoretical values obtained with the TALYS and CMPR codes in Fig. 23. A discrepancy between the theoretical calculations is clearly observed, and the experimental points are higher than the TALYS curve but lower than the CMPR curve with an exception at 19 MeV (this point is in good agreement with the TALYS calculation).

(c) ^{128}Te(γ, p)^{127}Sb reaction

The measured results for the ^{128}Te(γ, p)^{127}Sb reaction are compared with the theoretical values obtained with the TALYS and CMPR codes in Fig. 24. It is evident

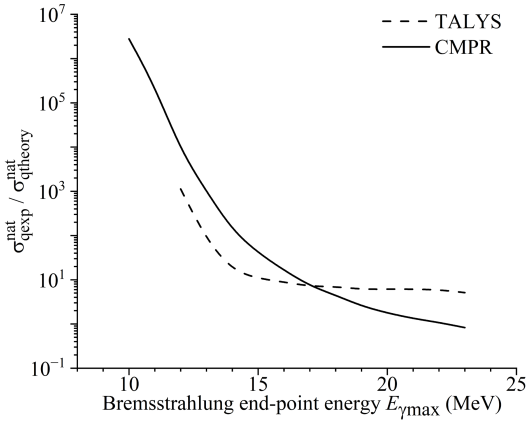

Fig. 22. Ratio of the cross section per equivalent quantum $\sigma^{nat}_{qexp}/\sigma^{nat}_{qtheory}$ for the ^{123}Te(γ, p)^{122}Sb reaction.

from Fig. 24 that the theoretical values based on the CMPR and the measured values in this study agree well in terms of both form and magnitude.

(d) ^{130}Te(γ, p)^{129}Sb reaction

Figure 25 displays the measured data and the computed values. A discrepancy between the theoretical cal-

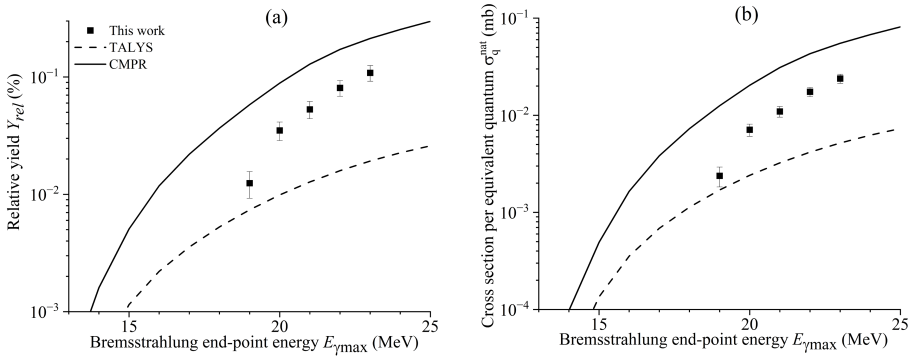

Fig. 23. Relative yields (a) and cross section per equivalent quantum (b) of the ^{125}Te(γ, p)^{124}Sb and ^{126}Te(γ, np)^{124}Sb reactions as functions of the bremsstrahlung end-point energy from this study (solid rectangles) and simulated values using the CMPR (solid lines) and TALYS code (dashed lines).

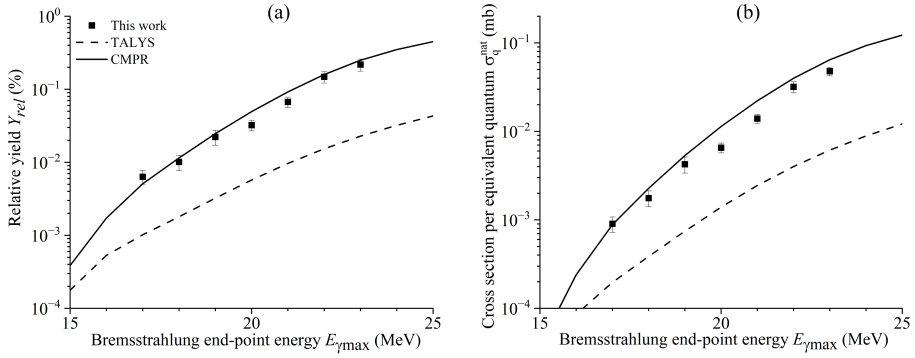

Fig. 24. Relative yields (a) and cross section per equivalent quantum (b) of the reaction ^{128}Te(γ, p)^{127}Sb as functions of the bremsstrahlung end-point energy from this study (solid rectangles) and simulated values using the CMPR (solid lines) and TALYS code (dashed lines).

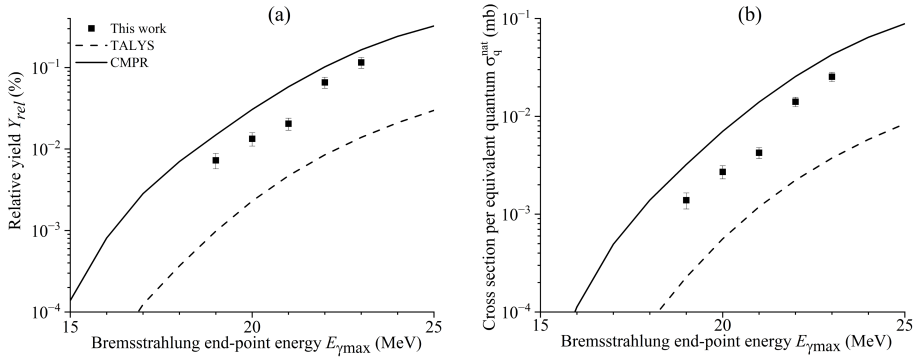

Fig. 25. Relative yields (a) and cross section per equivalent quantum (b) of the reaction ^{130}Te(γ, p)^{129}Sb as functions of the bremsstrahlung end-point energy from this study (solid rectangles) and simulated values using the CMPR (solid lines) and TALYS code (dashed lines).

culations is clearly observed, and the experimental points are higher than the TALYS curve but lower than the CMPR curve. The experimentally obtained results lie closer to the theoretical curve obtained from the CMPR.

C. Analysis of the results on (γ, *p*) reactions

The irradiation of the natural mixtures of Cd and Te allows us to study photonuclear reactions over a wide mass range of A=106−130. The cross section per equivalent quantum of the (γ, p) reaction in the case of monoisotopes σ_q calculated using CMPR and TALYS by applying Eq. (5) are contrasted against the experimental data in Fig. 26. The data in Fig. 26 show that the measured yields of the (γ, p) reactions on the isotopes ^{112,113,114,116}Cd and ^{128,130}Te agree within 30% with the results of the calculations based on the CMPR. The (γ, p) yields calculated using the TALYS code are underestimated with respect to the experimental data by one order of magnitude. The

reason behind this difference is that the TALYS code disregards the special features of the decay of the $T_>$ GDR component, where the decay through the proton channel to low-lying states of the final nucleus is forbidden by the isospin-selection rules. Thus, the $T_>$ states decay through the proton channel with a higher probability. The cross section per equivalent quantum calculations for the reactions ^{114}Cd(γ, p)^{113}Ag and ^{128}Te(γ, p)^{127}Sb using the TALYS parameters, models of the nuclear level densities and γ-ray strength functions, and accounting for isospin splitting in the CMPR are given in Appendix B.

The measured (γ, p) yields are a few percent of the (γ,n) yields for all nuclei, with the exception of the ^{106}Cd nucleus, for which the yield of the reaction ^{106}Cd(γ, p)^{105}Cd is commensurate with the yield of the reaction ^{106}Cd(γ, n)^{105}Cd, but this contradicts the results of the theoretical calculations in [24, 25]. The situation is unclear for the ^{123}Te(γ, p)^{122}Sb reaction. In all experiments, the spectra show a line at 564 keV. However, theoretical calculations using TALYS and CMPR are several orders of magnitude smaller.

For a more thorough analysis of the obtained results, the ratios between the reaction yields (γ,p) and (γ,n) were calculated for the nuclei ^{106}Cd (^{105}Ag/^{105}Cd), ^{116}Cd (^{115}Ag/^{115}Cd), ^{128}Te (^{127}Sb/^{127}Te), and ^{130}Te (^{129}Sb/^{129}Te). In addition, the ratios of the yields (γ, p)/(γ, n) were calculated for the nucleus ^{74}Se based on the experimental results in our previous study [40]. Figure 27(a) shows that the ratio between the reaction yields (γ, p) and (γ, n) depends on the electron energy of the accelerator. As shown in Fig. 27(a), the ratios of the yields (γ, p)/(γ, n) are almost equal to 1 for the bypassed nuclei ^{74}Se and ^{106}Cd. It can be seen that with the exception of the points for the nucleus ^{106}Cd, the experimental points are consistent with the calculated curves of the CMPR. In the case of ^{106}Cd (^{105}Ag/^{105}Cd), CMPR and TALYS cannot describe the experimental results. The reason for the observed discrepancy between theory and experiment may be explained by the fact that statistical models of photonuclear reactions do not consider the individual structural features of the Cd isotopes.

Figure 27(b) shows the ratios of the yields (γ, p)/(γ, n) as functions of the proton-neutron ratio N/Z at the electron energy of 23 MeV of the accelerator. The literature data were calculated using the experimentally measured reaction cross sections (γ, p) and (γ, n) on the nuclei ^{90}Zr [41–42], ^{89}Y [42–43], ^{103}Rh [1, 44], ^{112}Sn [45–46], and ^{160}Gd [47]. With the exception of the points at N/Z = 1.176 (^{74}Se) and 1.208 (^{106}Cd), the experimental points are consistent with the curve calculated using the CMPR.

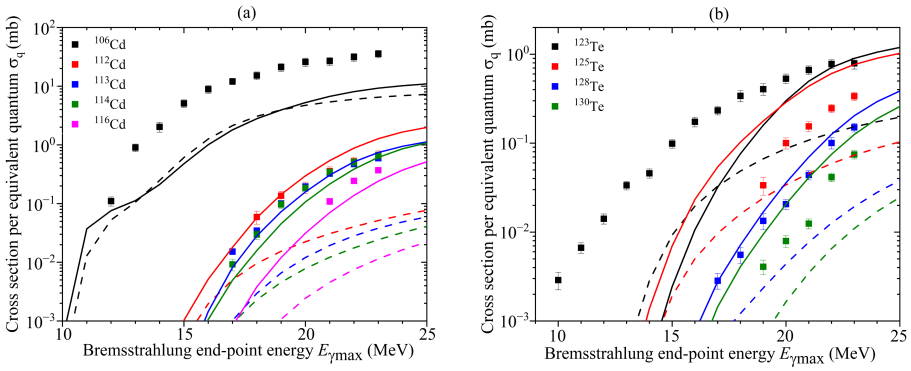

Fig. 26. (color online) Cross section per equivalent quantum of the (γ, p) reaction in the case of monoisotopes σ_q for the stable isotopes of cadmium (a) and tellurium (b).

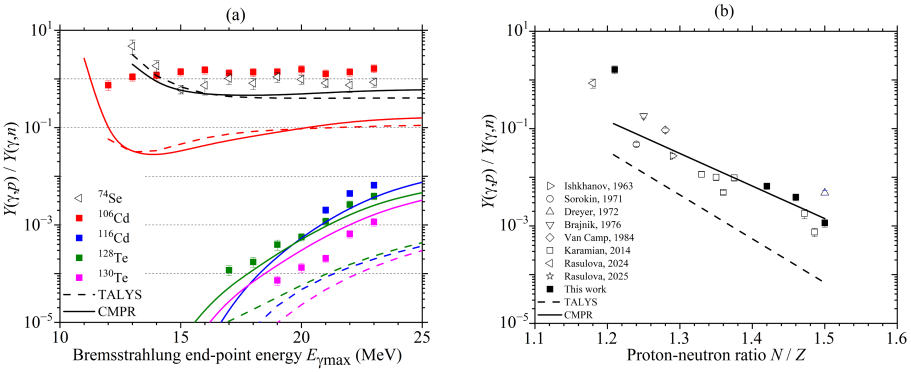

Fig. 27. (color online) Ratio of the reaction yields (γ, p)/(γ, n) as functions of: (a) the electron energy of the accelerator and (b) the proton-neutron ratio N/Z at the electron energy of 23 MeV of the accelerator.

The ratio of the yields (γ, p)/(γ, n) decreases with increasing proton-neutron ratio N/Z.

D. Isomeric ratios for the pairs ^{116}Cd(γ,n)$^{115\,m,g}$Cd, ^{120}Te(γ,n)$^{119\,m,g}$Te, ^{122}Te(γ,n)$^{121\,m,g}$Te and ^{130}Te(γ,n)$^{129\,m,g}$Te

Based on the measured experimental yields of the metastable and ground states from Tables 1−2 in Appendix 1, we obtained the isomeric yield ratio (IR=σ_h/σ_l) of ^{115g}Cd (nuclear spin=1/2$^+$) and ^{115m}Cd (nuclear spin=11/2$^-$) in the ^{nat}Cd(γ,n) reactions, which are given in Table 3 for various bremsstrahlung end-point energies. The photon induced isomeric ratios in this study and the literature data in the GDR region [7−15] are shown in Fig. 28(a). As seen in Fig. 28(a), the experimental isomeric ratios in the ^{116}Cd(γ, n) reaction are in agreement with the theoretical values. Furthermore, Fig. 28(a) shows that the isomeric ratios of ^{115m,g}Cd increase with increasing excitation energy.

In the experiments, we registered three isomeric pairs of tellurium, ^{119,121,129}Te. All isomeric states have the nuclear spin 11/2$^-$. Based on the measured experimental yields of the metastable and ground states, we obtained the isomeric yield ratio (IR=σ_h/σ_l) for each of them, as shown in Figs. 28(b), (c), (d), for various bremsstrahlung end-point energies.

Table 3. Isomeric ratios of the ^{116}Cd(γ,n)^{115}Cd and ^{nat}Te(γ,n)^{119,121,129}Te reactions at the bremsstrahlung end-point energies of 11−23 MeV from the present work

$E_{\gamma max}$/MeV	^{116}Cd(γ,n)^{115}Cd	^{120}Te(γ,n)^{119}Te	^{122}Te(γ,n)^{121}Te	^{130}Te(γ,n)^{129}Te
11				0.023 (4)
12	0.05 (1)			0.045 (8)
13	0.06 (1)	0.024 (6)	0.06 (1)	0.12 (2)
14	0.08 (1)	0.04 (1)	0.09 (1)	0.14 (2)
15	0.09 (1)	0.06 (1)	0.12 (2)	0.18 (3)
16	0.11 (2)	0.08 (1)	0.13 (2)	0.23 (3)
17	0.12 (2)	0.08 (1)	0.15 (2)	0.21 (4)
18	0.13 (2)	0.11 (2)	0.17 (3)	0.25 (4)
19	0.13 (2)	0.10 (2)	0.17 (3)	0.25 (4)
20	0.15 (2)	0.11 (2)	0.18 (3)	0.27 (4)
21	0.16 (2)	0.11 (2)	0.19 (3)	0.27 (4)
22	0.16 (2)	0.11 (2)	0.19 (3)	0.28 (4)
23	0.15 (2)	0.12 (2)	0.19 (3)	0.27 (4)

For the reaction ^{120}Te(γ, n)^{119}Te, the photon induced isomeric ratios in this study and the literature data in the GDR region [10, 19, 20] are shown in Fig. 27(b). As seen in Fig. 28(b), our experimental isomeric ratios in the

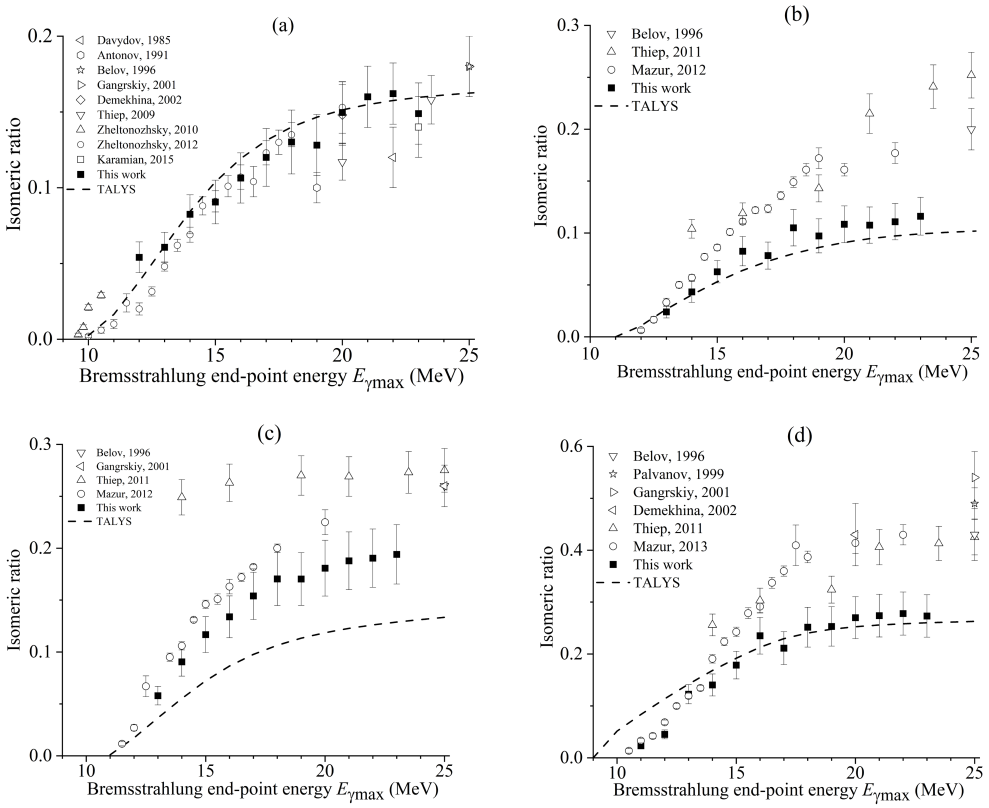

Fig. 28. Isomeric yield ratios of the pairs ^{116}Cd(γ, n)^{115m,g}Cd (a), ^{120}Te(γ, n)^{119m,g}Te (b), ^{122}Te(γ, n)^{121m,g}Te (c), and ^{130}Te(γ, n)^{129m,g}Te (d) as functions of the bremsstrahlung end-point energy from this study (solid squares), literature data, and simulated values using TALYS code (dashed lines).

^{120}Te(γ, *n*) reaction are in agreement with the TALYS curve. Starting from 15 MeV, a scatter is observed in our results and the literature data for the isomeric ratios. Moreover, the figure shows that the isomeric ratios of ^{119m,g}Te increase with increasing excitation energy.

For the reaction ^{122}Te(γ, *n*)^{121}Te, the photon induced isomeric ratios from this study and the literature data in the GDR region [10, 11, 19, 20] are shown in Fig. 28(c). As seen in Fig. 28(c), our experimental values of the isomeric ratios in the reaction ^{nat}Te(γ, *n*)^{121m,g}Te are consistent with the literature data, but they diverge from the TALYS curve from 11 MeV onward. Additionally, as the excitation energy increases, the isomeric ratios of ^{121m,g}Te rise, as shown in the figure.

For the reaction ^{130}Te(γ, *n*)^{129}Te, the photon-induced isomeric ratios from this study and the literature data in the GDR region [10−12, 17, 19, 21] are shown in Fig. 28(d). As seen in Fig. 28(d), our experimental isomeric ratios in the ^{130}Te(γ, *n*) reaction are in agreement with the TALYS curve. Starting from 14 MeV, a scatter is observed in our results and the literature data for the isomeric ratios. Furthermore, the figure shows that the isomeric ratios of ^{129m,g}Te increase with increasing excitation energy.

V. CONCLUSION

This study addressed the measurements of the relative yields and cross section per equivalent quantum for the photonuclear reactions on a natural mixture of cadmium and tellurium using bremsstrahlung end-point energies of 10 to 23 MeV. The bremsstrahlung photon flux was computed using the Geant4.11.1 code. The experimental results were compared with the calculations using the TALYS model with standard parameters and the CMPR. For the photoneutron reactions on the nuclei ^{112,116}Cd(γ, *n*) and ^{120,122,124,126,130}Te, a good agreement was observed between the experimental data and theoretical calculations.

The measured (γ, *p*) yields are a few percent of the (γ, *n*) yields for all nuclei, with the exception of the bypassed nucleus ^{106}Cd, for which the yield of the reaction ^{106}Cd(γ, *p*)^{105}Cd is commensurate with the yield of the reaction ^{106}Cd(γ, *n*)^{105}Cd, but this contradicts the results of the theoretical calculations. For the reaction ^{123}Te(γ, *p*)^{122}Sb, the experimental points are almost 100 times larger than the theoretical calculations.

On the heavy isotopes ^{112,113,114,116}Cd and ^{128,130}Te, the experimental results agree with the theoretical relative yields calculated using the CMPR. Including isospin splitting in the CMPR enables a much better description of the experimental data on the reactions with proton escape in the energy range from 12 to 23 MeV. Therefore, the consideration of isospin splitting is necessary for a more reasonable description of the GDR decay. The study of photonuclear reactions on cadmium and tellurium isotopes is important for understanding the formation and decay of the bypassed nuclei during nucleosynthesis.

ACKNOWLEDGMENT

The authors would like to thank the staff of the MT-25 microtron at the Flerov Laboratory of Nuclear Reactions, Joint Institute for Nuclear Research, for their cooperation in the realization of the experiments. The authors are grateful for the support from the National Research Foundation of South Africa in association with Joint Institute for Nuclear Research (Project No. 22, Radiochemistry, FLNR Part).

APPENDIX A: DATA SUPPORTING THE FINDINGS OF THIS ARTICLE

In this Appendix, the tabulated experimental results discussed in Sec. IV are presented.

Table A1. Experimental results of ^{nat}Cd(γ, *n*) and ^{nat}Cd(γ, *p*) reactions.

	^{nat}Cd(γ, *n*)											
$E_{\gamma max}$/MeV	^{106}Cd(γ, *n*)^{105}Cd		^{108}Cd(γ, *n*)^{107}Cd		^{110}Cd(γ, *n*)^{109}Cd		^{112}Cd(γ, *n*)^{111m}Cd		^{116}Cd(γ, *n*)^{115g}Cd		^{116}Cd(γ, *n*)^{115m}Cd	
	Y_{rel} (%)	σ_q^{nat} /mb	Y_{rel} (%)	σ_q^{nat} /mb	Y_{rel} (%)	σ_q^{nat} /mb	Y_{rel} (%)	σ_q^{nat} /mb	Y_{rel} (%)	σ_q^{nat} /mb	Y_{rel} (%)	σ_q^{nat} /mb
10							14 (2)	0.006 (1)	100 (11)	0.06 (1)		
11							6.2 (9)	0.007 (1)	100 (11)	0.12 (1)		
12	0.7 (1)	0.0018 (3)	1.9 (4)	0.006 (1)	44 (7)	0.13 (2)	6.0 (9)	0.015 (2)	95 (10)	0.27 (3)	5 (1)	0.015 (2)
13	1.9 (3)	0.010 (1)	3.1 (5)	0.017 (2)	50 (9)	0.27 (5)	6 (1)	0.034 (6)	94 (10)	0.50 (5)	6 (1)	0.031 (4)
14	3.1 (5)	0.022 (3)	5.0 (7)	0.035 (4)	88 (14)	0.61 (9)	12 (2)	0.082 (9)	92 (10)	0.64 (7)	8 (1)	0.053 (6)
15	3.3 (4)	0.045 (5)	5.3 (6)	0.073 (8)	91 (11)	1.2 (2)	12 (2)	0.16 (2)	92 (10)	1.3 (2)	8 (1)	0.11 (2)
16	3.4 (5)	0.072 (8)	6.1 (9)	0.13 (2)	89 (10)	1.9 (2)	8.7 (9)	0.19 (2)	90 (9)	1.9 (2)	10 (1)	0.20 (2)
17	4.6 (6)	0.11 (2)	6.4 (9)	0.16 (2)	96 (11)	2.4 (3)	13 (2)	0.32 (3)	89 (9)	2.2 (2)	11 (1)	0.26 (3)

Continued on next page

Table A1-continued from previous page

	^{nat}Cd(γ, *n*)											
$E_{\gamma max}$/MeV	^{106}Cd(γ, *n*)^{105}Cd		^{108}Cd(γ, *n*)^{107}Cd		^{110}Cd(γ, *n*)^{109}Cd		^{112}Cd(γ, *n*)^{111m}Cd		^{116}Cd(γ, *n*)^{115g}Cd		^{116}Cd(γ, *n*)^{115m}Cd	
	Y_{rel} (%)	σ_q^{nat} /mb	Y_{rel} (%)	σ_q^{nat} /mb	Y_{rel} (%)	σ_q^{nat} /mb	Y_{rel} (%)	σ_q^{nat} /mb	Y_{rel} (%)	σ_q^{nat} /mb	Y_{rel} (%)	σ_q^{nat} /mb
18	5.1 (7)	0.14 (2)	7 (1)	0.19 (2)	105 (13)	2.8 (4)	20 (3)	0.54 (6)	88 (9)	2.4 (2)	12 (2)	0.31 (4)
19	5.9 (8)	0.19 (2)	8 (1)	0.26 (3)	120 (19)	3.9 (5)	23 (3)	0.75 (8)	89 (9)	2.9 (3)	11 (2)	0.36 (4)
20	5.3 (8)	0.21 (2)	7 (1)	0.30 (3)	135 (23)	5.3 (7)	22 (3)	0.9 (1)	87 (9)	3.4 (3)	13 (2)	0.51 (6)
21	6.5 (9)	0.26 (3)	8 (1)	0.32 (3)	135 (22)	5.4 (7)	26 (4)	1.1 (1)	86 (9)	3.5 (4)	14 (2)	0.58 (7)
22	6.9 (9)	0.28 (3)	9 (1)	0.35 (4)	141 (22)	5.8 (7)	27 (4)	1.1 (1)	86 (9)	3.5 (4)	14 (2)	0.57 (7)
23	6.7 (9)	0.27 (3)	9 (1)	0.37 (4)	144 (22)	6.0 (7)	28 (4)	1.2 (1)	87 (9)	3.6 (4)	13 (2)	0.54 (7)

	^{116}Cd(γ, *n*)^{115}Cd		^{nat}Cd(γ, *p*)									
			^{106}Cd(γ, *p*)^{105}Ag		^{112}Cd(γ, *p*)^{111}Ag		^{113}Cd(γ, *p*)^{112}Ag		^{114}Cd(γ, *p*)^{113}Ag		^{116}Cd(γ, *p*)^{115}Ag	
10		0.06 (1)										
11		0.12 (1)										
12		0.28 (3)	0.5 (1)	0.0014 (2)								
13		0.53 (5)	2.1 (4)	0.011 (2)								
14		0.69 (7)	3.7 (8)	0.025 (5)								
15		1.4 (2)	4.6 (7)	0.06 (1)								
16		2.1 (2)	5.2 (9)	0.11 (2)								
17		2.5 (3)	6.1 (9)	0.15 (2)			0.07 (1)	0.0019 (2)	0.11 (3)	0.003 (1)		
18		2.7 (3)	7.0 (1.3)	0.19 (3)	0.5 (1)	0.014 (4)	0.16 (2)	0.0042 (4)	0.32 (6)	0.009 (2)		
19		3.2 (3)	8.0 (1.5)	0.26 (4)	1.0 (2)	0.033 (6)	0.38 (6)	0.012 (1)	0.9 (1)	0.028 (4)		
20		3.9 (4)	8.3 (1.6)	0.32 (5)	1.2 (3)	0.05 (1)	0.61 (9)	0.024 (3)	1.4 (2)	0.053 (7)		
21		4.0 (4)	8.3 (1.5)	0.33 (5)	2.1 (4)	0.08 (1)	0.98 (15)	0.039 (4)	2.4 (4)	0.098 (14)	0.20 (3)	0.008 (1)
22		4.1 (4)	9.6 (1.5)	0.39 (6)	3.1 (6)	0.13 (2)	1.4 (2)	0.058 (6)	3.6 (6)	0.15 (2)	0.44 (8)	0.018 (2)
23		4.2 (4)	11 (2)	0.44 (6)	3.8 (8)	0.16 (3)	1.7 (2)	0.073 (8)	4.5 (8)	0.19 (3)	0.66 (9)	0.028 (3)

Table A2. Experimental results of ^{nat}Te(γ, *n*) and ^{nat}Te(γ, *p*) reactions.

	^{nat}Te(γ, *n*) reactions															
$E_{\gamma max}$ /MeV	^{120}Te(γ, *n*)^{119g}Te		^{120}Te(γ, *n*)^{119m}Te		^{120}Te(γ, *n*)^{119}Te		^{122}Te(γ, *n*)^{121g}Te		^{122}Te(γ, *n*)^{121m}Te		^{122}Te(γ, *n*)^{121}Te		^{123}Te(γ, γ`)^{123m}Te + ^{124}Te(γ, *n*)^{123m}Te + ^{125}Te(γ, 2*n*)^{123m}Te		^{125}Te(γ, γ`)^{125m}Te + ^{126}Te(γ, *n*)^{125m}Te	
	Y_{rel} (%)	σ_q^{nat} /mb	Y_{rel} (%)	σ_q^{nat} /mb	Y_{rel} (%)	σ_q^{nat} /mb	Y_{rel} (%)	σ_q^{nat} /mb	Y_{rel} (%)	σ_q^{nat} /mb	Y_{rel} (%)	σ_q^{nat} /mb	Y_{rel} (%)	σ_q^{nat} /mb	Y_{rel} (%)	σ_q^{nat} /mb
10							0.11 (2)	0.0005 (1)			0.11 (2)	0.0005 (1)	0.43 (7)	0.0020 (2)	9 (2)	0.04 (1)
11	0.015 (2)	0.00013 (2)			0.015 (2)	0.00013 (2)	1.6 (2)	0.013 (1)			1.6 (2)	0.013 (2)	0.27 (4)	0.0023 (2)	9 (2)	0.07 (2)
12	0.058 (6)	0.00058 (6)			0.058 (6)	0.00058 (6)	3.0 (5)	0.030 3()			3.0 (5)	0.030 (3)	0.41 (6)	0.0041 (5)	10 (3)	0.13 (3)
13	0.15 (2)	0.0029 (3)	0.004 (1)	0.00007 (2)	0.15 (2)	0.003 (1)	5.5 (8)	0.11 (1)	0.32 (5)	0.006 (1)	5.8 (9)	0.12 (2)	0.9 (1)	0.019 (2)	11 (3)	0.21 (5)
14	0.13 (2)	0.0047 (5)	0.005 (1)	0.00020 (4)	0.13 (2)	0.005 (1)	4.4 (7)	0.17 (2)	0.40 (6)	0.015 (2)	4.8 (9)	0.18 (3)	1.0 (2)	0.038 (4)	11 (2)	0.41 (8)
15	0.13 (2)	0.009 (2)	0.008 (1)	0.0006 (1)	0.14 (2)	0.009 (2)	4.7 (7)	0.32 (3)	0.55 (8)	0.034 (4)	5.2 (9)	0.36 (5)	1.2 (2)	0.08 (1)	11 (2)	0.8 (2)
16	0.15 (2)	0.017 (2)	0.012 (2)	0.0014 (2)	0.16 (2)	0.018 (3)	5.2 (8)	0.61 (6)	0.7 (1)	0.08 (1)	5.9 (9)	0.7 (1)	1.6 (2)	0.19 (2)	11 (3)	1.3 3
17	0.14 (2)	0.021 (2)	0.011 (2)	0.0017 (2)	0.15 (3)	0.023 (4)	4.5 (7)	0.67 (7)	0.7 (1)	0.10 (1)	5.2 (9)	0.8 (1)	1.6 (2)	0.23 (2)	12 (2)	1.7 (3)
18	0.17 (3)	0.029 (3)	0.018 (3)	0.0031 (4)	0.18 (3)	0.033 (5)	4.9 (9)	0.87 (9)	0.8 (1)	0.15 (2)	5.8 (9)	1.0 (2)	1.9 (3)	0.34 (3)	13 (3)	2.4 (4)
19	0.17 (3)	0.034 (4)	0.017 (3)	0.0033 (4)	0.19 (4)	0.037 (6)	5.1 (9)	1.0 (1)	0.9 (1)	0.17 (2)	6 (9)	1.1 (2)	2.0 (3)	0.38 (4)	13 (3)	2.5 (4)
20	0.18 (3)	0.037 (4)	0.019 (3)	0.0040 (5)	0.20 (4)	0.041 (7)	5.5 (8)	1.1 (1)	1.0 (2)	0.20 (2)	6.5 (9)	1.3 (2)	2.3 (3)	0.46 (5)	13 (3)	2.7 (5)

Continued on next page

Table A2-continued from previous page

$E_{\gamma\max}$ /MeV	$^{\rm nat}$Te(γ, *n*) reactions															
	^{120}Te(γ, *n*)^{119g}Te		^{120}Te(γ, *n*)^{119m}Te		^{120}Te(γ, *n*)^{119}Te		^{122}Te(γ, *n*)^{121g}Te		^{122}Te(γ, *n*)^{121m}Te		^{122}Te(γ, *n*)^{121}Te		^{123}Te(γ, γ`)^{123m}Te + ^{124}Te(γ, *n*)^{123m}Te + ^{125}Te(γ, 2*n*)^{123m}Te		^{125}Te(γ, γ`)^{125m}Te + ^{126}Te(γ, *n*)^{125m}Te	
	$Y_{\rm rel}$ (%)	$\sigma_q^{\rm nat}$ /mb	$Y_{\rm rel}$ (%)	$\sigma_q^{\rm nat}$ /mb	$Y_{\rm rel}$ (%)	$\sigma_q^{\rm nat}$ /mb	$Y_{\rm rel}$ (%)	$\sigma_q^{\rm nat}$ /mb	$Y_{\rm rel}$ (%)	$\sigma_q^{\rm nat}$ /mb	$Y_{\rm rel}$ (%)	$\sigma_q^{\rm nat}$ /mb	$Y_{\rm rel}$ (%)	$\sigma_q^{\rm nat}$ /mb	$Y_{\rm rel}$ (%)	$\sigma_q^{\rm nat}$ /mb
21	0.19 (3)	0.039 (4)	0.020 (3)	0.0042 (5)	0.21 (4)	0.043 (7)	5.7 (8)	1.2 (1)	1.1 (2)	0.22 (2)	6.8 (9)	1.4 (2)	2.4 (4)	0.50 (5)	14 (3)	2.9 (5)
22	0.19 (3)	0.040 (4)	0.021 (3)	0.0045 (5)	0.21 (4)	0.045 (7)	5.7 (8)	1.2 (1)	1.1 (2)	0.23 (2)	6.8 (9)	1.4 (2)	2.5 (4)	0.54 (6)	14 (3)	3.0 (4)
23	0.19 (3)	0.042 (4)	0.022 (3)	0.0048 (5)	0.21 (4)	0.046 (7)	5.6 (8)	1.2 (1)	1.1 (2)	0.23 (2)	6.7 (9)	1.4 (2)	2.6 (4)	0.56 (6)	15 (3)	3.1 (5)
	$^{\rm nat}$Te(γ, *p*) reactions															
	^{128}Te(γ, *n*)^{127}Te		^{130}Te(γ, *n*)^{129g}Te		^{130}Te(γ, *n*)^{129m}Te		^{130}Te(γ, *n*)^{129}Te		^{123}Te(γ, *p*)^{122}Sb		^{125}Te(γ, *p*)^{124}Sb		^{128}Te(γ, *p*)^{127}Sb		^{130}Te(γ, *p*)^{129}Sb	
10	41 (6)	0.19 (2)	100 (15)	0.47 (5)				0.47 (5)	0.005 (1)	0.00003 (1)						
11	57 (7)	0.47 (5)	98 (10)	0.81 (9)	2.0 (4)	0.019 (3)		0.83 (9)	0.007 (1)	0.00006 (1)						
12	62 (7)	0.59 (7)	96 (10)	0.95 (9)	4.0 (8)	0.046 (7)		1.0 (1)	0.013 (2)	0.00013 (2)						
13	56 (7)	1.1 (2)	89 (10)	1.8 (2)	11 (2)	0.22 (2)		2.0 (2)	0.015 (2)	0.00030 (4)						
14	60 (7)	2.2 (3)	88 (10)	3.3 (3)	12 (2)	0.46 (5)		3.8 (4)	0.011 (2)	0.00041 (5)						
15	58 (8)	3.9 (4)	85 (10)	5.8 (6)	15 (2)	1.0 (1)		6.8 (7)	0.013 (2)	0.0009 (1)						
16	58 (8)	6.6 (7)	81 (10)	9.4 (9)	19 (3)	2.2 (2)		11 (1)	0.014 (2)	0.0016 (2)						
17	53 (8)	7.6 (9)	83 (10)	12 (1)	17 (3)	2.8 (3)		15 (2)	0.015 (2)	0.0021 (2)			0.006 (1)	0.0009 (1)		
18	58 (8)	10 (1)	80 (11)	14 (1)	20 (3)	3.5 (4)		17 (2)	0.017 (3)	0.0030 (4)			0.010 (2)	0.0018 (3)		
19	56 (9)	11 (1)	80 (11)	15 (2)	20 (3)	3.9 (4)		19 (2)	0.019 (3)	0.0036 (5)	0.012 (3)	0.0024 (5)	0.022 (5)	0.004 (1)	0.007 (1)	0.0014 (2)
20	57 (9)	12 (1)	79 (10)	16 (2)	21 (3)	4.3 (4)		20 (3)	0.023 (4)	0.005 (1)	0.035 (6)	0.007 (1)	0.032 (5)	0.006 (1)	0.013 (2)	0.0027 (4)
21	57 (9)	12 (1)	79 (10)	16 (2)	21 (3)	4.4 (4)		20 (3)	0.028 (4)	0.006 (1)	0.053 (9)	0.011 (1)	0.07 (1)	0.014 (2)	0.020 (3)	0.0042 (5)
22	56 (9)	12 (1)	78 (10)	17 (2)	22 (3)	4.7 (5)		22 (3)	0.032 (5)	0.007 (1)	0.08 (1)	0.017 (2)	0.15 (3)	0.032 (4)	0.07 (1)	0.014 (2)
23	56 (9)	12 (1)	79 (10)	17 (2)	21 (3)	4.7 (5)		22 (3)	0.032 (6)	0.007 (1)	0.11 (2)	0.024 (3)	0.22 (4)	0.048 (5)	0.11 (2)	0.025 (3)

APPENDIX B: TALYS PARAMETERS AND ACCOUNTING FOR ISOSPIN SPLITTING IN CMPR

The essential components of the TALYS calculations for photonuclear reaction cross sections are the nuclear level densities and γ-ray strength functions. The cross sections of the reactions were computed in this study using TALYS 2.0 with standard parameters. For the reactions ^{114}Cd(γ, *p*)^{113}Ag and ^{128}Te(γ, *p*)^{127}Sb, the effects of altering various input options were examined, including the level densities (Constant Temperature + Fermi gas model, Back-shifted Fermi gas Model, Generalized Superfluid Model, Skyrme-Hartree-Fock-Bogolyubov level densities from numerical tables, Skyrme-Hartree-Fock-Bogolyubov combinatorial level densities from numerical tables, Temperature-dependent Gogny-Hartree-Fock-Bogolyubov combinatorial level densities from numerical tables) and γ-strength functions (Kopecky-Uhl generalized Lorentzian, Brink-Axel Lorentzian, Hartree-Fock BCS tables, Hartree-Fock-Bogoliubov tables, Goriely's hybrid model, Goriely T-dependent HFB, T-dependent RMF, Gogny D1M HFB+QRPA, Simplified Modified Lorentzian Model, Skyrme HFB+QRPA).

Using these options, the cross section per equivalent quantum for the reactions ^{114}Cd(γ, *p*)^{113}Ag and ^{128}Te(γ, *p*)^{127}Sb are displayed in Figures B1 and B2. Changing the parameters LD 1−6 and GSF 1−10 gives 60 different results for the theoretical σ(*E*) and $\sigma_q^{\rm nat}(E)$. As seen in Fig. B1 and Fig. B2, changes in these input options have no effect on the TALYS results. Thus, it is confirmed that the difference between the TALYS and CMPR results is due to the consideration of isospin splitting in the CMPR. A brief description of isospin splitting is given below.

In the nuclei with $N \neq Z$, upon absorption of the electric dipole γ photons, two branches of the GDR are excited, $T_< = T_0$ and $T_> = T_0 + 1$, where $T_0 = \frac{|N-Z|}{2}$ [48]. Fig. B3 shows the excitations of the isospin components $T_<$ and $T_>$ of the GDR in the initial nucleus (*N*, *Z*) and their decay according to the proton (*N*, *Z* − 1) and neutron (*N* − 1, *Z*) channels. From Fig. B3, it can be observed that the decay of the excited GDR states with isospin $T_> = T_0 + 1$ according to the neutron channel to low-lying states $T = T_0 - 1/2$ with neutron emission is forbidden, which leads to an increase in the reaction cross section (γ, *p*) and a maximum shift of the reaction cross section (γ, *p*) with respect to the reactions (γ, *n*) toward higher energies in the

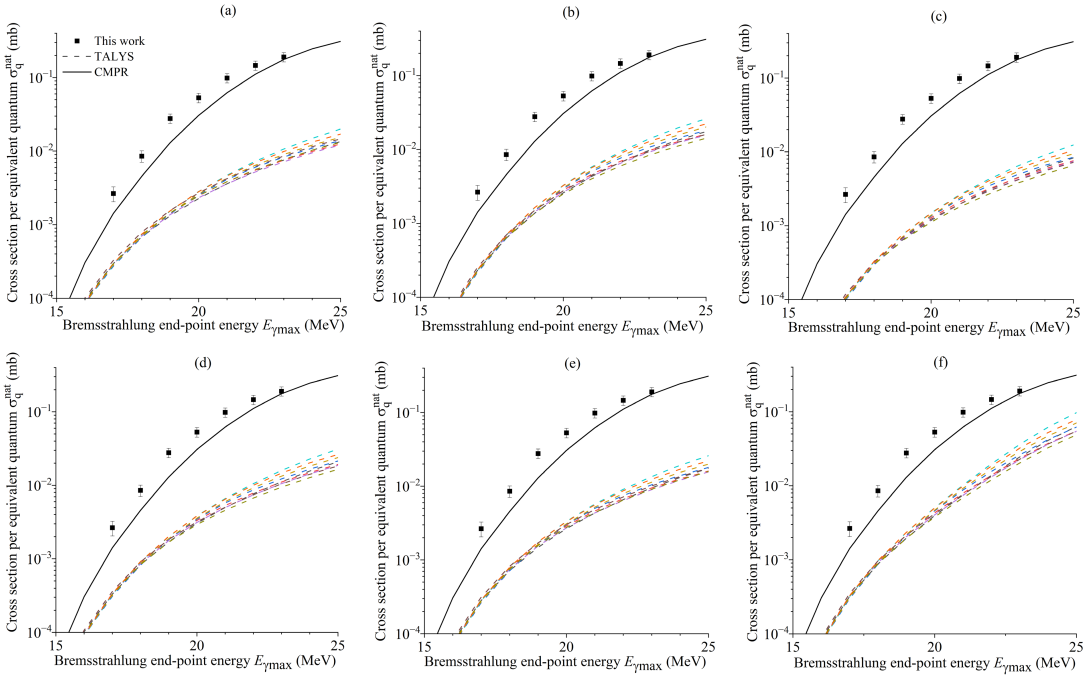

Fig. B1. (color online) Cross sections per equivalent quantum $\sigma_q^{nat}(E)$ for the ^{114}Cd(γ, p)^{113}Ag reaction calculated with the TALYS code for six level density models *LD*1-*LD*6 (a-f) and ten gamma strength functions (dashed lines) as well as simulated values using the CMPR (solid lines).

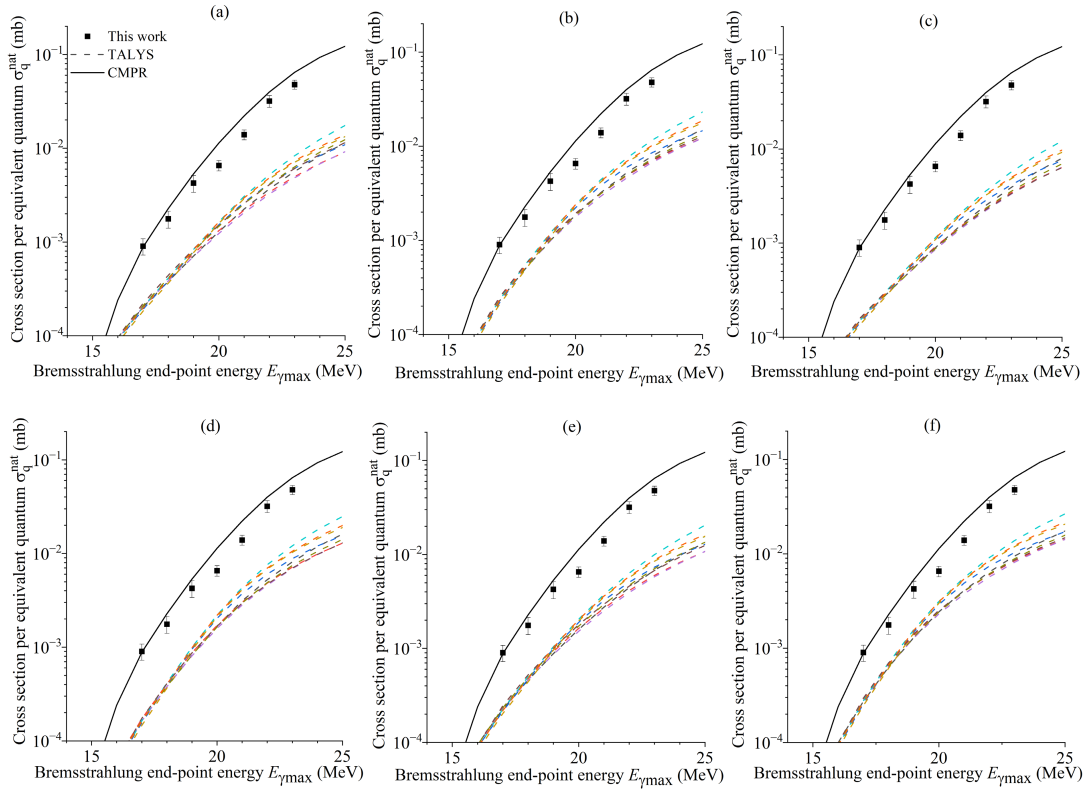

Fig. B2. (color online) Cross sections per equivalent quantum $\sigma_q^{nat}(E)$ for the ^{128}Te(γ, p)^{127}Sb reaction calculated with the TALYS code for six level density models *LD*1-*LD*6 (a-f) and ten gamma strength functions (dashed lines) as well as simulated values using the CMPR (solid lines).

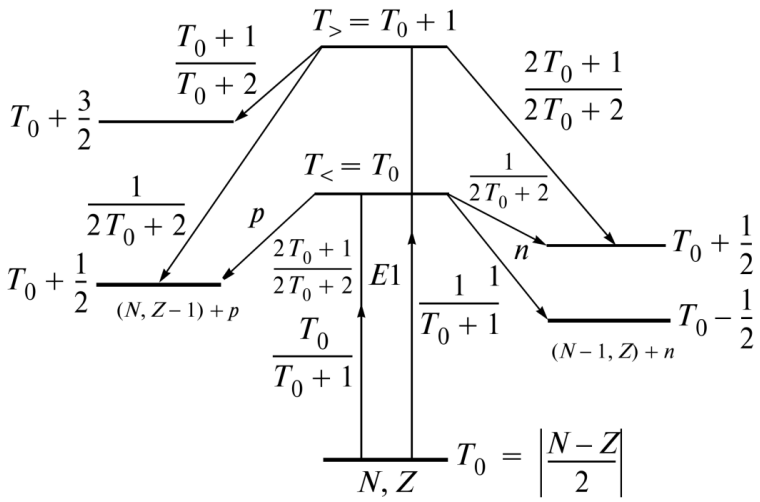

Fig. B3. Scheme of excitation of states $T_<$ and $T_>$ in the nucleus (N, Z) and their decay along the proton channel (N, $Z-1$) and neutron channel ($N-1$, Z).

Table B1. CMPR results for GDR isospin energy splitting, integral cross sections $\sigma_<^{\rm int}$ and $\sigma_>^{\rm int}$ of the isospin component reactions (γ, s*n*) and (γ, s*p*), and ratio of the reaction cross sections $\frac{\sigma_>^{\rm int}}{\sigma_<^{\rm int}}$, calculated based on CMPR.

$^{\rm nat}$Cd								
A	T_0	$E(T_>)$-$E(T_<)$	(γ, *sn*)			(γ, *sp*)		
			$\sigma_<^{\rm int}$/(MeV·mb)	$\sigma_>^{\rm int}$/(MeV·mb)	$\frac{\sigma_>^{\rm int}}{\sigma_<^{\rm int}}$	$\sigma_<^{\rm int}$/(MeV·mb)	$\sigma_>^{\rm int}$/(MeV·mb)	$\frac{\sigma_>^{\rm int}}{\sigma_<^{\rm int}}$
106	5	3.40	1405	42	0.03	193	210	1.09
108	6	3.89	1560	42	0.03	92	156	1.70
110	7	4.36	1648	45	0.03	58	112	1.92
111	7.5	4.59	1716	66	0.04	57	99	1.73
112	8	4.82	1711	49	0.03	47	77	1.64
113	8.5	5.04	1778	69	0.04	46	60	1.30
114	9	5.26	1772	50	0.03	41	48	1.17
116	10	5.69	1823	46	0.03	36	27	0.75
$^{\rm nat}$Te								
A	T_0	$E(T_>)$-$E(T_<)$	(γ, *sn*)			(γ, *sp*)		
			$\sigma_<^{\rm int}$/(MeV·mb)	$\sigma_>^{\rm int}$/(MeV·mb)	$\frac{\sigma_>^{\rm int}}{\sigma_<^{\rm int}}$	$\sigma_<^{\rm int}$/(MeV·mb)	$\sigma_>^{\rm int}$/(MeV·mb)	$\frac{\sigma_>^{\rm int}}{\sigma_<^{\rm int}}$
120	8	4.50	1819	43	0.02	63	108	1.71
122	9	4.92	1891	46	0.02	40	74	1.85
123	9.5	5.12	1964	63	0.03	39	62	1.59
124	10	5.32	1943	47	0.02	34	47	1.38
125	10.5	5.52	2015	49	0.02	35	49	1.40
126	11	5.71	1995	42	0.02	30	31	1.03
128	12	6.09	2043	36	0.02	28	18	0.64
130	13	6.46	2084	28	0.01	27	12	0.44

nucleus (N, Z).

The value of isospin splitting of the GDR is determined by the following relation [49]:

$$\Delta E = E(T_>) - E(T_<) = \frac{60}{A}(T_0 + 1). \tag{B1}$$

The ratio of the probabilities of the excitation of states

$T_>$ and $T_<$ is described by the following relation [50]:

$$\frac{\sigma(T_>)}{\sigma(T_<)} = \frac{1}{T_0}\frac{1-1.5T_0A^{-2/3}}{1+1.5A^{-2/3}}. \quad \text{(B2)}$$

Table B1 shows the values of the energy of the GDR isospin energy splitting calculated based on the relations (1) for isotopes ^{nat}Cd and ^{nat}Te. In addition, Table B1 contains the integral cross sections $\sigma^{int}_<$ and $\sigma^{int}_>$ of the isospin component reactions (γ, sn) = (γ, n) + (γ, np) + (γ, 2n) and (γ, sp) = (γ, p) + (γ, np) + (γ, 2p) in the energy region below 40 MeV and ratio of the reaction cross sections $\frac{\sigma^{int}_>}{\sigma^{int}_<}$, calculated based on the CMPR for isotopes ^{nat}Cd and ^{nat}Te. Table B1 shows that for ^{nat}Cd, the growth in the mass number A from 106 to 116 results in an increase in the isospin energy splitting by ≈2.29 MeV. For ^{nat}Te, the growth in A from 120 to 130 leads to an increase in energy splitting by the value ≈2.16 MeV. The isospin splitting leads to the shift in the proton cross section of the relatively neutron on the side of the high energy.

References

[1] A. Lepretre, H. Beil, R. Bergere *et al.*, Nuc. Phys. A **219**, 39 (1974)
[2] S. A. Karamian, Physics of Atomic Nuclei **77**, 1429 (2014)
[3] S. A. Karamian, J. J. Carroll, N. V. Aksenov, Phys. Atom. Nuclei **78**, 757 (2015)
[4] S. S. Belyshev, B. S. Ishkhanov, V. N. Orlin, Phys. Atom. Nuclei **76**, 931 (2013)
[5] S. S. Belyshev, B. S. Ishkhanov, A. A. Kuznetsov *et al.*, Phys. Atom. Nuclei **77**, 809 (2014)
[6] S. S. Belyshev, A. A. Kuznetsov, K. A. Stopani *et al.*, Phys. Atom. Nuclei **79**, 641 (2016)
[7] Muhammad Nadeem, Md. Shakilur Rahman, Muhammad Shahid *et al.*, Chin. Phys. C **45**, 124002 (2021)
[8] M. G. Davydov, V. G. Magera, A. V. Trukhov *et al.*, Atom. Energy, **58**, 47 (1985).
[9] A. D. Antonov, N. P. Balabanov, A. G. Belov *et al.*, Isomeric ratios in the reaction (γ, n) for nuclei in the range A = 70−125, in *Proc. Int. Conf. on Nuclear Physics (91MINSK)* (Inst. Nucl. Problems, Belarusian State Univ., Minsk, 1991), p. 286.
[10] A. G. Belov, Yu. P. Gangrsky, A. P. Tonchev *et al.*, Phys. Atom. Nucl. **59**, 553 (1996).
[11] Yu. P. Gangrskiy, P. Zuzaan, N. N. Kolesnikov *et al.*, Bull. Russ. Acad. Sci. Phys. **65**, 121 (2001).
[12] N. A. Demekhina, A. S. Danagulyan, G. S. Karapetyan *et al.*, Phys. Atom. Nuclei **65**, 365 (2002)
[13] T. D. Thiep, T. T. An, N. T. Khai, *et al.*, Phys. Part. Nuclei Lett. **6**, 126 (2009)
[14] V. O. Zheltonozhsky, A. M. Savrasov, Bull. Russ. Acad. Sci. Phys. **74**, 829 (2010)
[15] V. O. Zheltonozhsky, V. M. Mazur, D. M. Symochko *et al.*, UJP, **56**, 443 (2011).
[16] A. Leprêtre, H. Beil, R. Bergére *et al.*, Nucl. Phys. A, **258**, 350 (1976)
[17] S. R. Palvanov, O. Razhabov, Atomic Energy, **87**, 75 (1999).
[18] T. V. Poltorzhytska, G. F. Pitchenko, Ukr. J. Phys. **29**, 162 (2011).
[19] T. D. Thiep, T. T. Thiep, P. V. Cuong *et al.*, Radioanal Nucl Chem **289**, 637 (2011)
[20] V. M. Mazur, Z. M. Bigan, D. M. Symochko *et al.*, PPN/L, **9**, 248 (2012).
[21] V. M. Mazur, D. M. Symochko, Z. M. Bigan *et al.*, Phys. Rev. C, **87**, 044604 (2013).
[22] V. M. Mazur, Z. M. Bigan, P. S. Derechkey *et al.*, YFE, **20**, 228 (2019).
[23] H. Morinaga, Phys. Rev. **97**, 444 (1955).
[24] A. Koning, S. Hilaire, S. Goriely. TALYS-2.0: A Nuclear Reaction Program, User Manual, 2025. https://nds.iaea.org/talys/tutorials/talys.pdf
[25] B. S. Ishkhanov, V. N. Orlin, Phys. Atom. Nucl. **78**, 557 (2015)
[26] T. A. Aweda, O. Ikotun, T. Mastren *et al.*, Medicinal Chemistry Communication **4**(6), 1015 (2013)
[27] M. Prata, D. Alloni, P. De Felice *et al.*, Eur. Phys. J. Plus **129**, 1 (2014)
[28] M. Ballan, M. Tosato, M. Verona, et. al., Applied Radiation and Isotopes, **164**, 109258 (2020).
[29] L. Morselli, A. Donzella, A. Arzenton, et. al., Applied Radiation and Isotopes **197**, 110798 (2023).
[30] O. D. Maslov, S. N. Dmitriev, Use of MT-25 microtron for scientific and applied investigations, https://inis.iaea.org/collection/NCLCollectionStore/_Public/35/022/35022466.pdf
[31] S. S. Belyshev, A. N. Ermakov, B. S. Ishkhanov *et al.*, Nucl. Instrum. Meth. Phys. Res. A **745**, 133 (2014).
[32] S. C. Fultz, R. L. Bramblett, J. T. Caldwell *et al.*, Phys. Rev. **133**, B1149 (1964)
[33] V. V. Varlamov, A. I. Davydov, M. A. Makarov *et al.*, Bulletin of the Russian Academy of Sciences: Physics, **80**, 317 (2016)
[34] S. Agostinelli, J. Allison, K. Amako *et al.*, Nucl. Instr. Meth. Phys. Res. A. **506** 250 (2003)
[35] B. S. Ishkhanov, A. A. Kuznetsov, Moscow Univ. Phys. Bull. , **68**, 279 (2013).
[36] S. S. Belyshev, K. A. Stopani, S. Yu. Troschiev *et al.*, Moscow Univ. Phys. Bull. , **66**, 363 (2011).
[37] J. Frana, J. Radioanal. Nucl. Chem. **257**(3), 583 (2003)
[38] Nudat 3.0, National Nuclear Data Center, Brookhaven National Laboratory, available from http://www.nndc.bnl.gov/nudat3/
[39] M. J. Berger, S. M. Seltzer, Phys. Rev. C, **2**, 621 (1970)
[40] F. A. Rasulova et. al., Chin. Phys. C **48**, 024002 (2024)
[41] D. Brajnik et. al., Physical Review C **13**, 1852 (1976)
[42] A. Lepretre et. al., Nuclear Physics A **175**, 609 (1971)
[43] E. Van Camp et. al., Physical Review C **30**, 1182 (1984)
[44] B. S. Ishkhanov et. al., Zh. Eksp. Teor. Fiz. **45**, 38(1963)
[45] Yu. I. Sorokin, V. A. Khrushchev, B. A. Yuryev, Yadernaya fizika **14**, 1118 (1971)
[46] V. V. Varlamov et. al., Bull. Acad. Sci. **74**, 833 (2010)
[47] F. Dreyer, H. Dahmen, J. Staube *et al.*, Nuclear Physics A **192**, 433 (1972)
[48] B. S. Ishkhanov and I. M. Kapitonov, *Giant dipole resonance in atomic nuclei: history of the prediction, discovery and exploration of the unique phenomenon. 75 years of the research* (Moscow: LENAND, 2021).
[49] R. O. Akyuz and S. Fallieros,, Phys. Rev. Lett. , **27**, 1016 (1971).
[50] B. Goulard and S. Fallieros, Can. J. Phys. , **45**, 3221 (1967).